Design and analysis of an aluminum F-shape bridge railing and median barrier

Malcolm H. Ray, Ph.D., P.E.
Elisa Oldani

Department of Civil and Environmental Engineering
Worcester Polytechnic Institute
Worcester, MA 01609

10 May 2004

Abstract

This report describes the design and analysis of an extruded aluminum truss-work bridge railing for NCHRP Report 350 test levels three and four conditions. Two versions of the barrier are examined: an F-shape aluminum parapet bridge railing and a similar F-shape aluminum median barrier. The objective of this research is to determine if the barriers will pass the NCHRP Report 350 full-scale crash tests for test levels three and four by using the nonlinear dynamic finite element program LS-DYNA. A subsequent AASHTO LRFD analysis supported the LS-DYNA result. The design documented in this report was found to be of comparable strength to other F-shaped bridge railings so that successful crash test results are highly likely.

Background

There is a long history of successful crash test performance with a variety of F-shape railings made using reinforced concrete. [1] [2] The barriers discussed in this report use the same F-shape profile that has been successfully tested before in the referenced research projects. Reinforced concrete barriers attached to a bridge deck behave essentially as rigid barriers so the primary issue to be considered is, are ultimate strengths of the F-shape parapet bridge railing and the F-shape aluminum median barrier equal to or greater than the reinforced concrete or steel variations of the barrier. If the aluminum F-shape barriers are shown to be at least as strong as the tested reinforced concrete barrier systems, it can be inferred that the aluminum barriers would likewise result in good crash test performance. In essence, prior crash testing has demonstrated that a rigid F-shape barrier results in acceptable test level four performance therefore any F-shape barrier will result in similar crash test results as long as the structural response is essentially rigid (i.e., there are no major deformations). With this in mind, the objective of this project was to compare the strength of the F-shape aluminum parapet bridge railing and the F-shape median barrier to the known crash test performance of other F-shape barriers to determine if the aluminum barriers are at least as strong as the reinforced concrete F-shaped barriers. Additionally, the likely performance of the aluminum F-shape barriers was assessed in nonlinear dynamic finite element simulations for the Report 350 Test 3-11 conditions (i.e., the pickup truck test) to determine the likely result of a full-scale crash test.[3] Following the dynamic analysis for test level three, an LRFD analysis corresponding to test level four was performed according to the procedure outlined in section 13 of the AASHTO LRFD Bridge Specification.[4]

Barrier Description

Two versions of an aluminum bridge railing will be discussed in this report: a parapet and a median barrier configuration. Both use extruded 6063-T6 aluminum truss-work panels as primary load bearing elements. The following sections provide more detailed descriptions of the two barriers and their components.

Parapet Bridge Railing

The aluminum parapet bridge railing, shown in Figure 1, is an 856-mm (34-inch) high F-shape barrier made up of (1) a base plate, (2) a post, (3) a lower truss-core extruded panel, (4) an upper truss-core extruded panel, (5) a top cap, (6) backing plates and (7) a variety of toe clips and other fasteners. The various components are interlocked with each other and secured using stainless steel cap screws.

The base plate, shown in Figure 2, provides a connection between the bridge deck and the post and lower truss-core panel of the bridge railing. The base plate is made using 6061-T6 aluminum alloy and is fastened to the deck using two one-inch diameter A325 galvanized steel bolts in the front and two M16 (5/8-in diameter) bolts in the rear of each base plate. The bolts are threaded into an epoxy insert in the bridge deck. M24 (one-inch diameter) bolts in the front resist the overturning moment of the post whereas the M16 (5/8-inch) bolts in the rear serve primarily an alignment purpose. The base plate is welded to the post along the web of the post as described below.

The post, shown in Figures 2 and 4, is extruded using 6061-T6 aluminum alloy. The shape of the post was modified during the project to ensure that the compression flange (i.e., the rear flange) did not buckle in an impact. Figure 4 also shows the inertial properties and a cross-section plot of the new post geometry. The web of the post is welded to the base plate shown in Figure 3 which is in turn bolted to the bridge deck using two M24 (one-inch diameter) A325 structural steel bolts.

When the structure is loaded, the flexural moment is transferred to the deck of the bridge through a triangular truss composed of the lower truss-core panel, the base plate and the back flange of the post (see Figure 1). The aluminum post initially loads in bending but it is quickly restrained by the triangular truss formed with the lower panel. In particular, the lower panel loads in tension while the post and the base plate are compressed. The upper part of the barrier (i.e., the upper truss-core panel shown in Figure 6) is loaded in bending as a whole system. The outer skin of the upper panel is loaded in tension while the rear flange of the post is in compression. The neutral axis of the system is located somewhere between the panel and the rear flange of the post, therefore, the front flange of the post is mainly loaded in shear, transferred through the upper clamp bar. Since the base of the posts is not significantly loaded in bending, only the web of the posts is welded to the base plate. Not welding the flanges avoids heat-effecting the base of the posts.

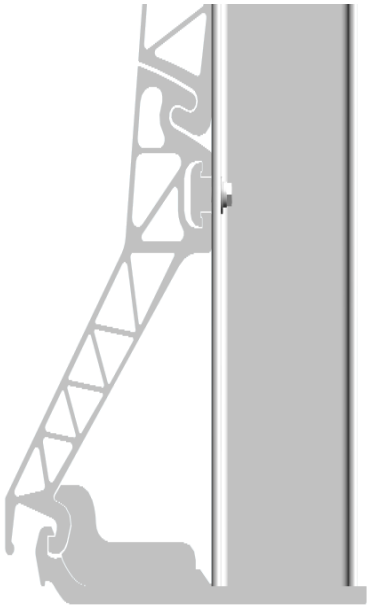

Figure 1. Base support triangle formed by the lower truss-core panel, the base plate and the rear flange of the post.

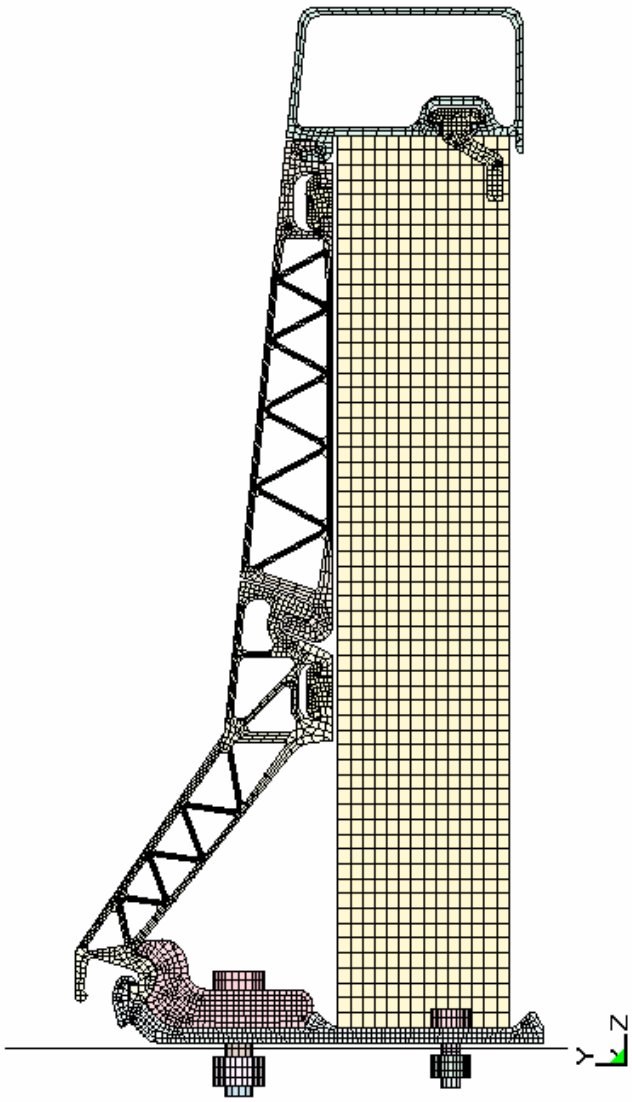

Figure 2. Finite element model of the aluminum parapet bridge railing.

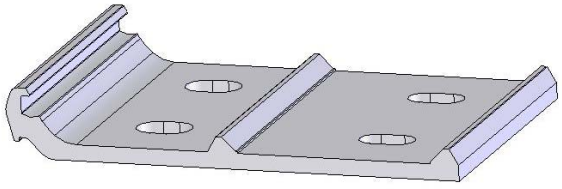

Figure 3. Three-dimensional model of the aluminum bridge parapet base plate.

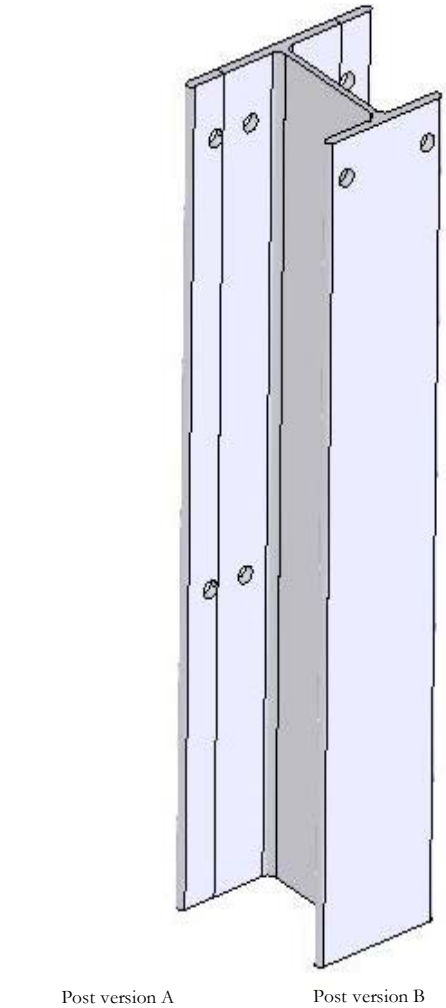

	Post version A	Post version B
Area [mm^2]	4007.22	5009.28
Perimeter [mm]	960.59	1028.88
Radii of giration x [mm^2]	44.84	50.01
Radii of giration y [mm^2]	79.13	90.18
Jx [mm^4]	8.02E+06	1.25E+07
Jy [mm^4]	1.67E+07	2.17E+07

Figure 4. Three-dimensional model, cross-section view and inertial properties of the aluminum bridge parapet post.

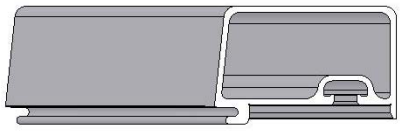

Top Rail	
Area	4752.67
Centroid coordinate, Cs	797.873
Centroid coordinate, Ct	113.634
Second Moment of Inertia, Iss	2.26E+07
Second Moment of Inertia, Itt	9.01E+06
Polar Moment of Inertia, Ir	3.16E+07

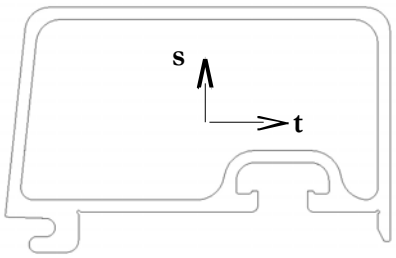

Figure 5. Three-dimensional model, cross-section view and inertial properties of the aluminum bridge parapet top rail.

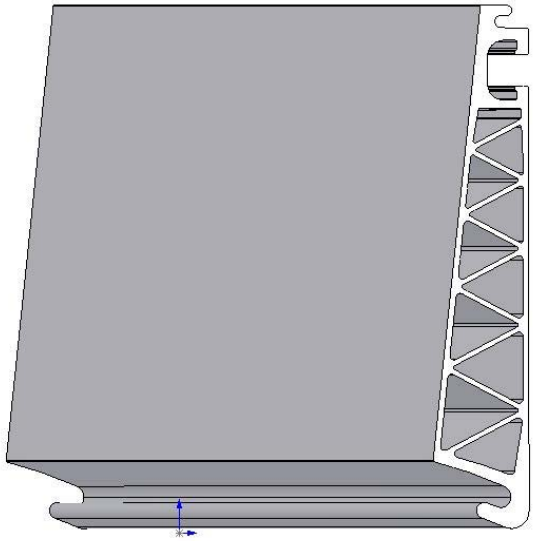

Upper Panel	
Area	8560.56
Centroid coordinate, Cs	534.398
Centroid coordinate, Ct	205.242
Second Moment of Inertia, Iss	3.95E+06
Second Moment of Inertia, Itt	1.40E+08
Polar Moment of Inertia, Ir	1.44E+08

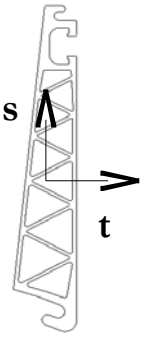

Figure 6. Three-dimensional model, cross-section view and inertial properties of the upper truss-core panel of the aluminum bridge parapet.

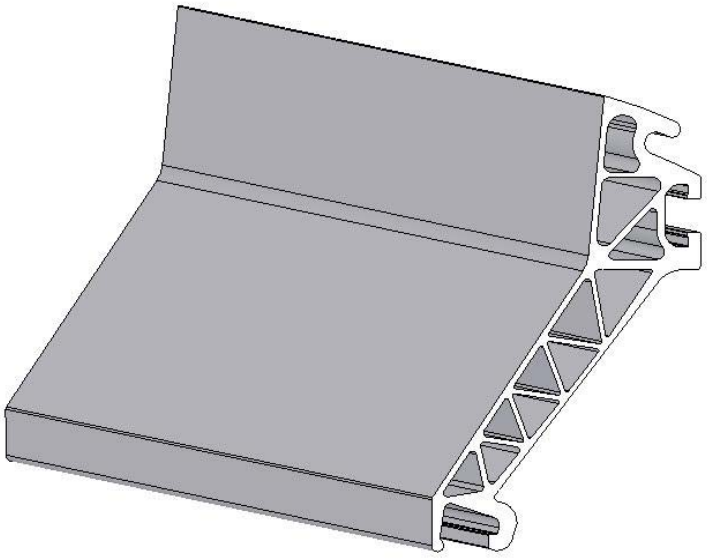

Lower Panel	
Area	9542.06
Centroid coordinate, Cs	218.143
Centroid coordinate, Ct	270.698
Second Moment of Inertia, Iss	3.50E+07
Second Moment of Inertia, Itt	1.00E+08
Polar Moment of Inertia, Ir	1.35E+08

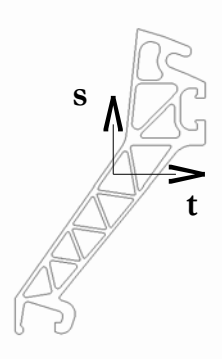

Figure 7. Three-dimensional model, cross-section view and inertial properties of the lower truss-core panel of the aluminum bridge parapet.

The top cap, shown in Figure 5, is extruded using 6063-T6 aluminum alloy. The top cap was modeled using a length of 6350-mm but it would generally be manufactured in lengths of 6 to 7 m. The top cap interlocks with the upper truss-core panel with an 18-8 stainless steel bolt and clamp bar and is secured to the top of the post with a steel cap screw. The structural function of the top rail is preventing the upper panel from bowing between the posts. It acts as a longitudinal beam, reacting to the longitudinal flexural moments that the external loads generate in the upper panel.

The upper truss-core panel, shown in Figure 6, is extruded using 6063-T6 aluminum alloy. The panel was modeled using a length of 6350-mm but it would generally be manufactured in the range of 6 to 7 m. The upper truss-core panel interlocks with the shape of the lower truss-core panel and the ridge top. The upper clamp bar fastens the upper edge of the upper truss-core panel to the post and backing plate using two 18-8 stainless steel bolts.

The lower truss-core panel, shown in Figure 7, is extruded using 6063-T6 aluminum alloy. The panel was also modeled using a length of 6350-mm but it would generally be manufactured in lengths of 6 to 7 m. The lower panel interlocks with the shape of the base plate on the lower edge and the upper truss-core panel on the upper edge. The lower clamp bar fastens the upper edge of the lower truss-core panel to the post using four 18-8 stainless steel bolts. The lower clamp bar attaches the lower truss-core panel to the backing plate at mid-span locations using only two stainless steel bolts.

The backing plates are located at midspan between two posts. Shorter base plates combined with

standard toe clips are also positioned at the same locations. First the base plates are installed on the deck of the bridge, followed by toe clips and posts, then a series of top rails are fixed to the posts. The top rail serves as a hanger to position a series of upper panels that are attached to the posts with clamp bars. The bottom panel is then positioned on the post bases and the bottom of the toe clips, rotated into place and interlocked with the upper panels.

Median Barrier

The aluminum median barrier, shown in Figure 8, is constructed in a similar manner to the parapet version described in the last section. The median barrier is a 356-mm (34-inch) high two-faced F-shape barrier made up of (1) a base plate, (2) a shear beam, (3) two lower truss-core extruded panels, (4) two upper truss-core extruded panels, (5) a top cap, (6) backing plates and (7) a variety of toe clips and other fasteners. The various components are interlocked with each other and secured using stainless steel cap screws. The base plate and shear beam are shown in Figures 9 and 10 and the top rail is shown in Figure 11. The lower and upper truss-core panels are the same as those described in the last section and shown in Figures 6 and 7.

Dynamic Analysis for Test Level Three

Background

In general, the Federal Highway Administration (FHWA) has required that bridge railings be evaluated in full-scale crash tests since 1986. A memorandum from the FHWA dated 16 May 2000 outlines a procedure for analyzing untested bridge rail configurations that are similar to tested systems.[5] The procedure was developed by the State of Colorado and is outlined in a 21 July 1998 document that is attached to the FHWA memorandum. Basically, the procedure involves the following syllogism: if a particular untested bridge railing can be shown to have the same ultimate strength as a geometrically similar bridge railing that has passed the Report 350 full-scale crash tests, then it can be inferred that the untested railing would also have passed the Report 350 full-scale crash tests. Stated more explicitly for the case of a rigid concrete barrier, the syllogism is:

- If a bridge railing:
  – Remains rigidly connected to the bridge deck during and after an impact and
  – The barrier structure is essentially undamaged,
- Then the bridge railing can be considered rigid.
- And if two bridge railings have the same shape and are essentially rigid,
- Then they should experience similar impact performance in the corresponding Report 350 tests.

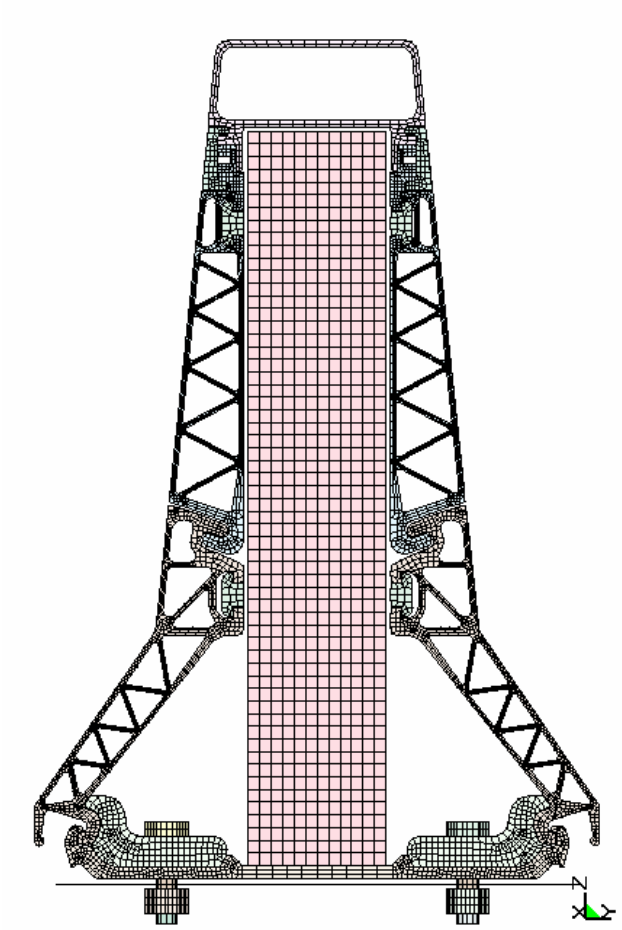

Figure 8. Finite-element model of an aluminum F-shape barrier.

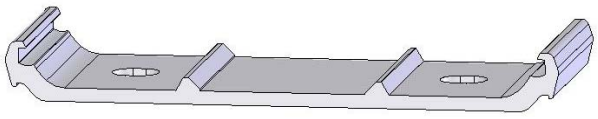

Figure 9. Three-dimensional model of the aluminum median barrier base plate.

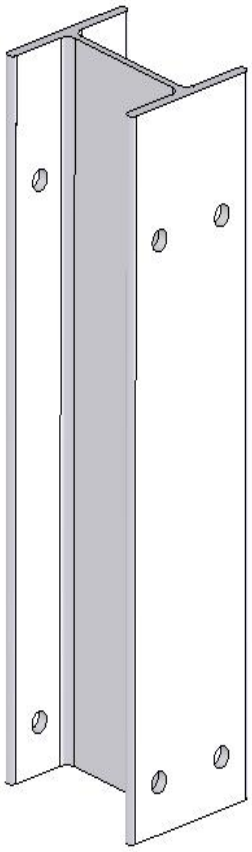

Shear Beam	
Area	3278.27
Second Moment of Inertia, Izz	13.63E+06
Second Moment of Inertia, Iyy	3.08E+06
Polar Moment of Inertia, Ir	5.01E+03

Figure 10. Three-dimensional model, cross-section and inertial properties of the aluminum median barrier shear beam.

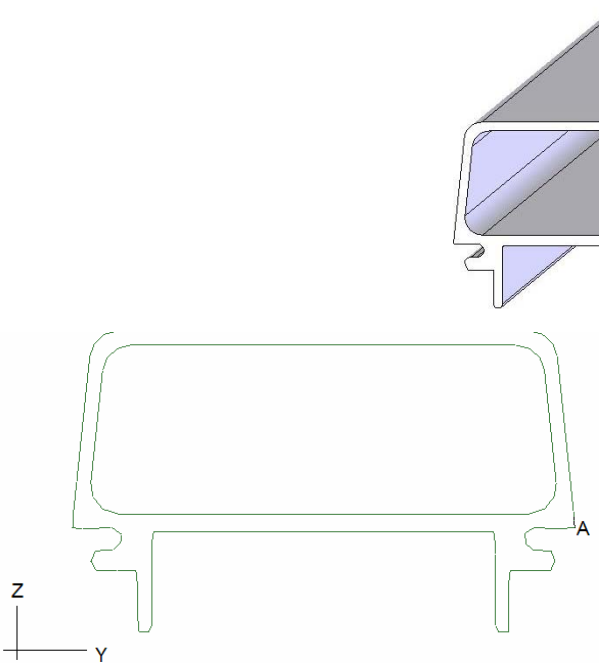

Top Rail	
Area	5135.8
Centroid coordinate, Cz	5061.48
Centroid coordinate, Cy	27.23
Second Moment of Inertia, Izz	30.84E+06
Second Moment of Inertia, Iyy	8.53E+06
Polar Moment of Inertia, Ir	5.01E+03

Figure 11. Three-dimensional model of the aluminum median barrier top rail.

This procedure was used to (1) determine the loads on a rigid F-shape concrete bridge railing usually considered to satisfy Report 350 test level four and (2) apply those same loads to an aluminum F-shape bridge railing to determine if the aluminum barrier responds in an essentially rigid manner. If the F-shape barrier does not experience excessive deformations under the loadings observed in a rigid F-shape barrier test, the response of the vehicle and its occupant can be assumed to be identical. Since the rigid concrete F-shape barrier passed the test level three and four criteria it can therefore be assumed that the aluminum F-shape barrier would likewise pass.

A dynamic analysis of the aluminum parapet and median barriers was performed using the finite element program LS-DYNA. The purpose of the analysis was to predict the performance of the two aluminum barrier systems in Report 350 Test 3-11 crash tests (i.e., the 2000-kg pickup truck striking the barrier at 100 km/hr and 25 degrees). A detailed finite element model of the barrier was developed and an already-developed finite element model of a 2000-kg pickup truck was used for this analysis. The analysis was performed using the program LS-DYNA.

Loads on F-shape barriers in Test 3-11

While a reinforced concrete F-shape bridge railing rigidly cast into the bridge deck is considered a test-level three barrier, no tests could be found in the roadside safety literature that exactly match Test 3-11 (i.e., a 2000-kg full-size pickup truck striking the barrier at a 25 degree angle at 100 km/hr). The reason for this is that most bridge rail testing was performed prior to the publication of NCHRP Report 350 according to the AASHTO bridge railing testing procedure.

An 810-mm (32-inch) tall reinforced concrete F-shape bridge railing was tested using the old AASHTO Bridge Specification criteria at Texas Transportation Institute (TTI) and the results are reported in both a TRB paper and an FHWA report.[6] [1] The AASHTO Bridge Specification PL-2 pickup truck test is similar to NCHRP Report 350 Test 3-11 except a 20 rather than 25 degree impact angle is used and the truck weight is 5,400 lbs rather than 4,500 lbs. The 810-mm (32-inch) tall F-shape, however, is considered to satisfy the Report 350 requirements since it also passes the higher level AASHTO PL-3 test criteria. If it can be demonstrated that the aluminum F-shape barriers can provide the same ultimate strength as the tested reinforced concrete F-shape barrier, then this should

Test Parameter	Test 7069-4		Simulation	
Test Vehicle				
Type	81 Chevrolet PU		C2500	
Mass	2470	kg	2408	kg
Impact Conditions				
Velocity	105.2	km/h	105.2	km/hr
Angle	20.4	deg	20.4	deg
Exit Conditions				
Velocity	91.6	km/hr	86.6	km/hr
Angle	7.4	deg	8.0	deg
Vehicle Accelerations (50 msec averages)				
Longitudinal	4.7	g's	8.2	g's
Lateral	13.1	g's	13.9	g's
Occupant Impact Velocity (OIV)				
Longitudinal	3.8	m/s	5.1	m/s
Lateral	7.3	m/s	7.4	m/s
Occupant Ridedown Acceleration (ORA)				
Longitudinal	1.2	g's	5.1	g's
Lateral	5.9	g's	15.2	g's

Table 1. Comparison of TTI Test 7069-4 and the finite element simulation of PL-2 test conditions.

form a basis for FHWA acceptance according to the 16 May 2000 FHWA Memorandum.

Estimating the loads experienced by a rigid F-shape barrier under Test 3-11 conditions, therefore, is a little more complicated than it would be if there were a full-scale test of a reinforced concrete F-shape bridge railing available. Since there is no such test available, a finite element analysis of the AASHTO PL-2 test was performed to compare the results with the crash test. The F-shape was modeled by using a surface of rigid (i.e., non-deformable) shells in the geometry of the F-shape barrier. A C2500 pickup truck model with fully functioning suspension, steering and tire models was used as the vehicle model.[7 8] The vehicle was set up initially for Report 350 testing so its mass was 2000 kg corresponding to the Report 350 test conditions. Additional mass was added to the model to ballast the model up to 2408 kg, as close to the 2450 kg AASHTO specifications as could be achieved while also balancing the rotatary moments of inertia.

The finite element simulation was then run at exactly the same speed and angle as the TTI test. The results are summarized in Table 1 and in Figures 12 and 13. As shown in the sequential photographs in Figures 12 and 13, the overall qualitative response of the vehicle in the finite element simulation was very similar to the actual full-scale crash test. Figure 12 shows a downstream view of the crash event and Figure 13 shows an overhead view of the event. Table 1 shows the quantitative parameters calculated by the TRAP program to evaluate full-scale crash tests. As shown in Table 1, the finite element simulation redirected the vehicle at almost the same exit angle but the vehicle was traveling 5 km/hr slower when it lost contact in the simulation than in the full-scale test. This is also reflected in the other parameters where the vehicle 50-msec average, occupant impact velocity and occupant ridedown velocity are all a little higher in the simulation for the longitudinal direction than in the full-scale test. This is a result of the barrier-vehicle friction being higher in the simulation than in the test. It would be possible to "tweak" the friction coefficients such that exactly the same values were obtained but the simulation values shown are more conservative (i.e., they estimate higher than actual loadings) so it was decided to keep the usual values. The values for the vehicle 50-msec average acceleration and occupant impact velocity in the lateral direction were nearly identical between the test and simulation indicating that the lateral loading is accurately represented by the finite element model. The lateral occupant ridedown acceleration was much higher in the simulation. This corresponded to a very high "tail slap" event in the simulation when the rear of the vehicle struck the barrier. Since the finite element simulation over-predicts the responses, the simulation yields conservative estimates of the barrier loading which is desirable from a design perspective.

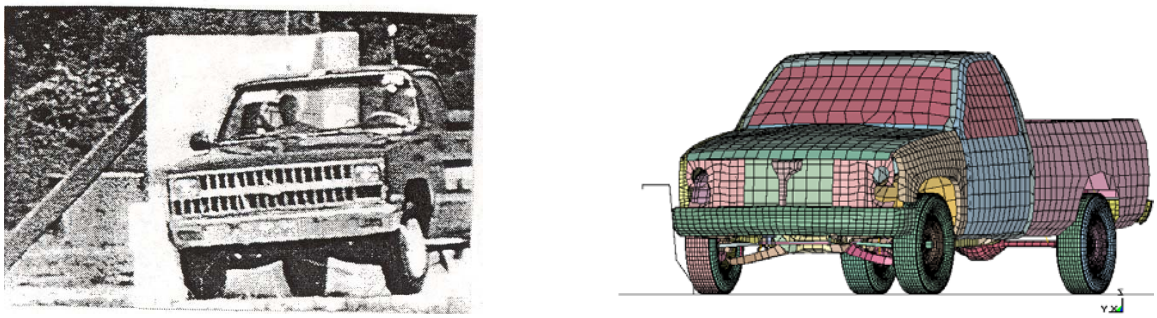

t = 0.000 sec.

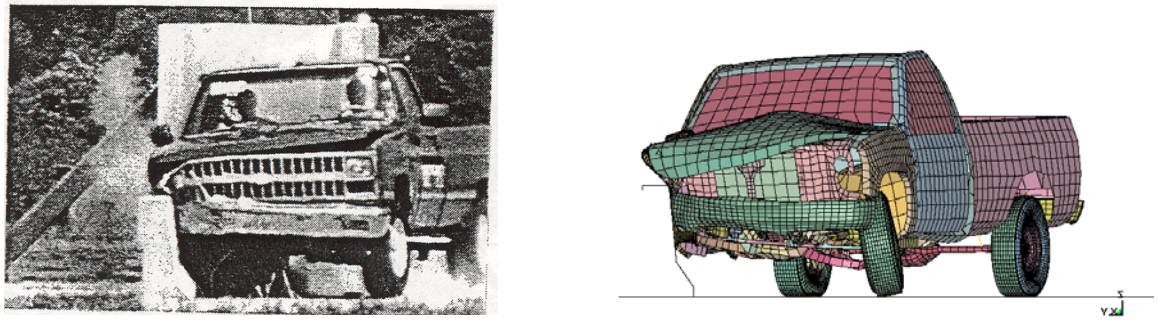

t = 0.051 sec.

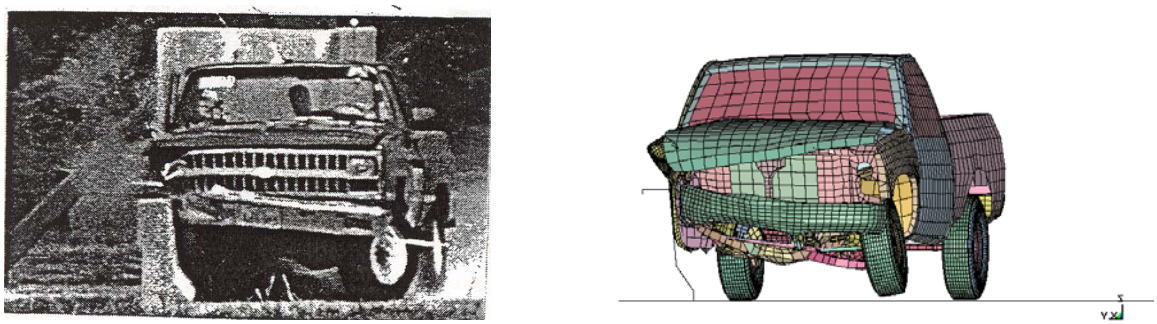

t = 0.099 sec.

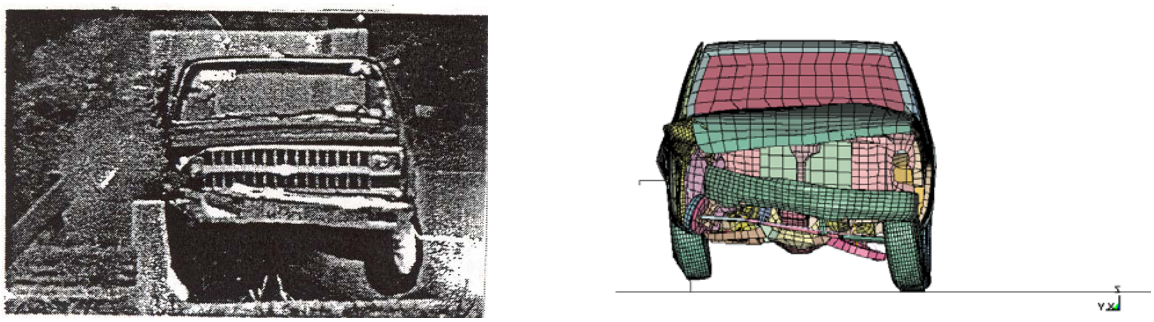

t = 0.150 sec.

Figure 12. Downstream view comparison of AASHTO PL-2 full-scale crash and a finite element simulation of an impact with a rigid F-shape bridge railing.

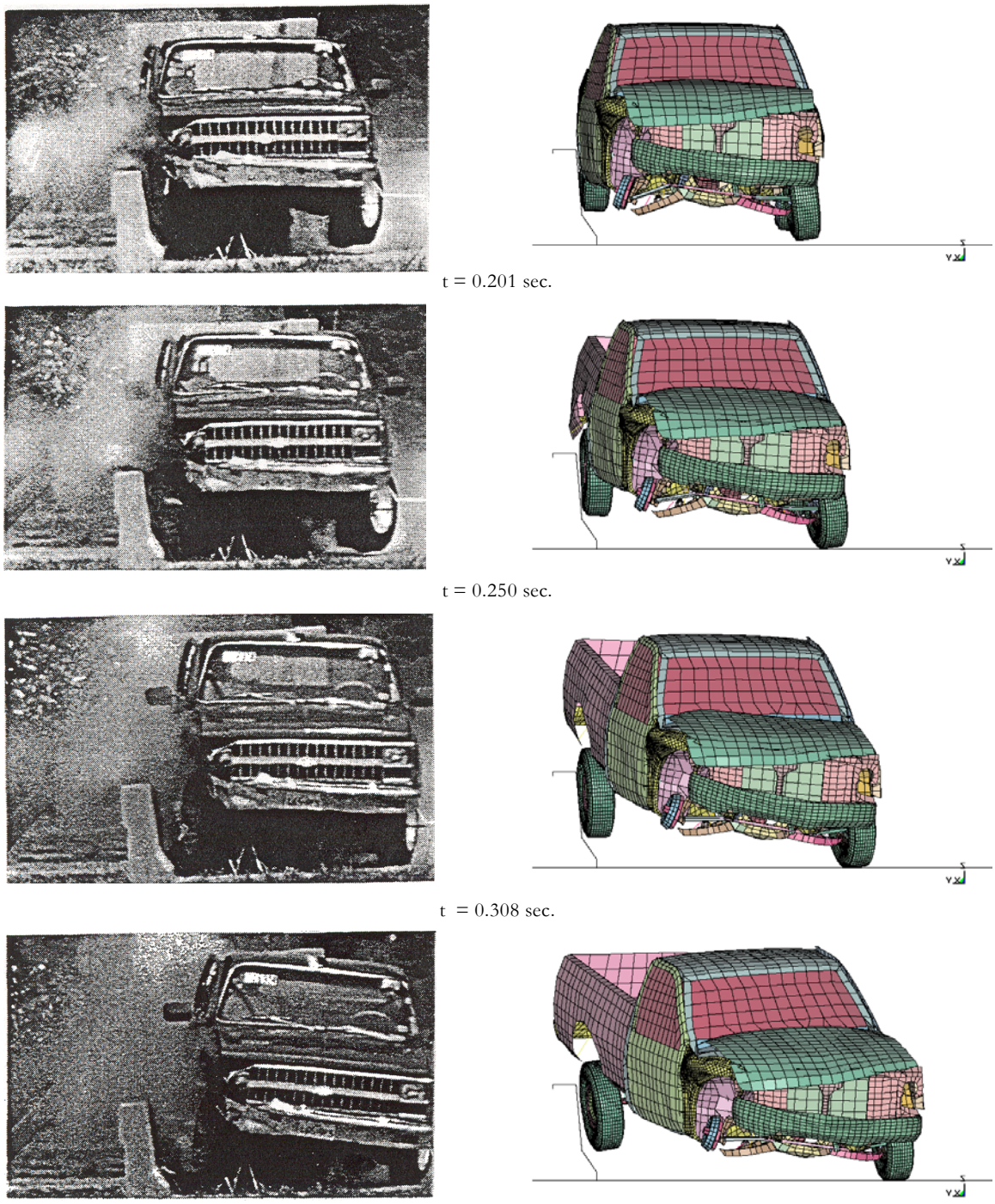

Figure 12. Downstream view comparison of AASHTO PL-2 full-scale crash and a finite element simulation of an impact with a rigid F-shape bridge railing (continued).

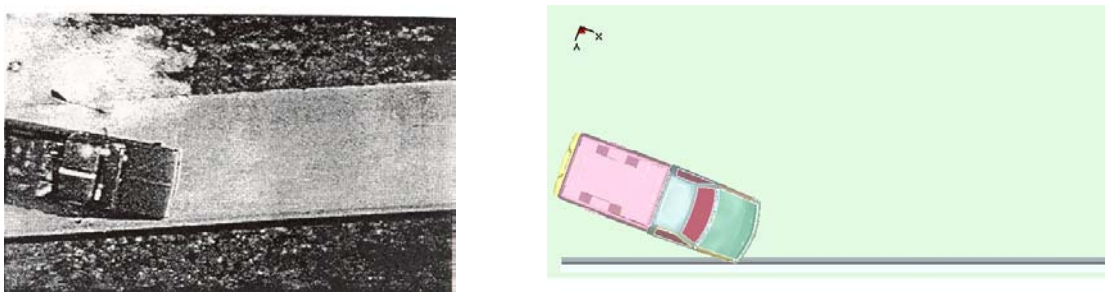

t = 0.000 sec.

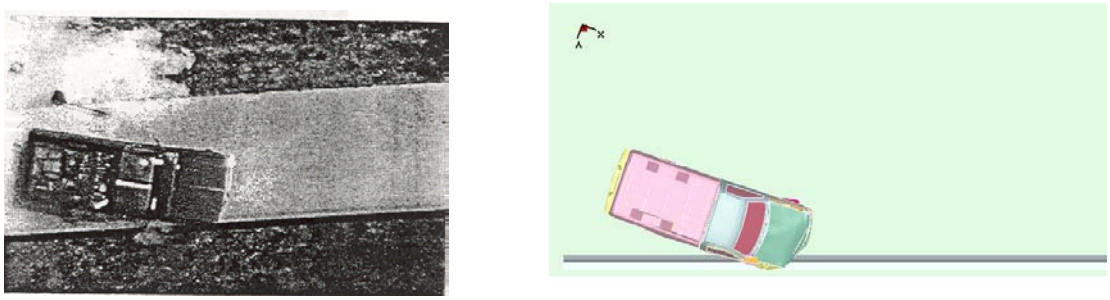

t = 0.051 sec.

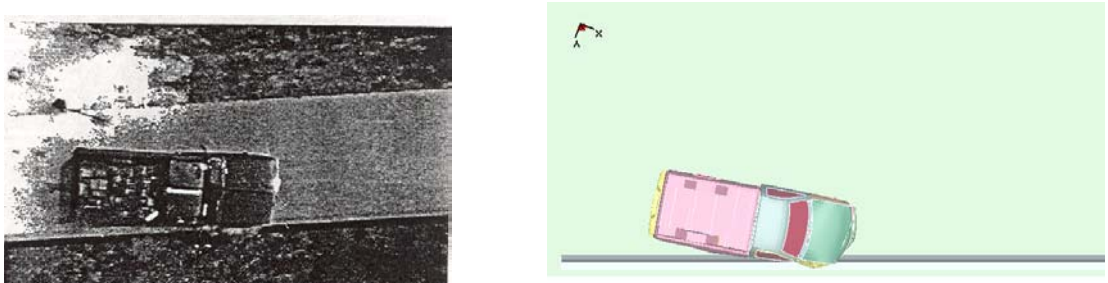

t = 0.099 sec.

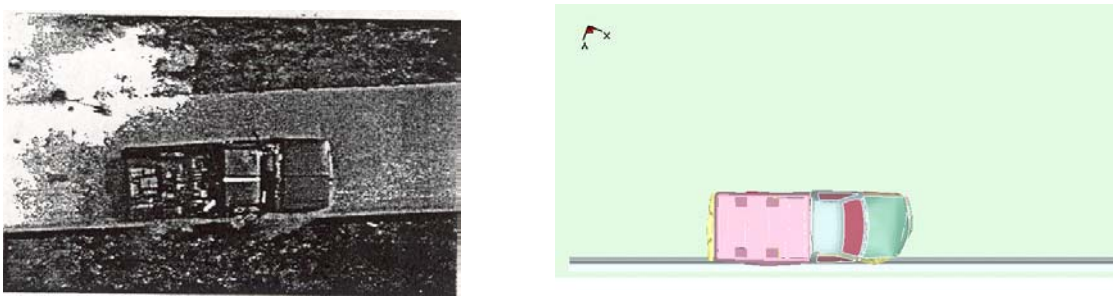

t = 0.150 sec.

Figure 13. Overhead comparison of AASHTO PL-2 full-scale crash and a finite element simulation of an impact with a rigid F-shape bridge railing.

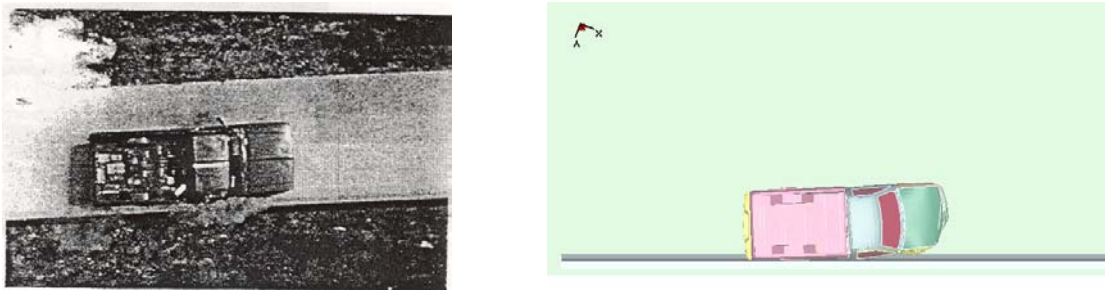

t= 0.201 sec.

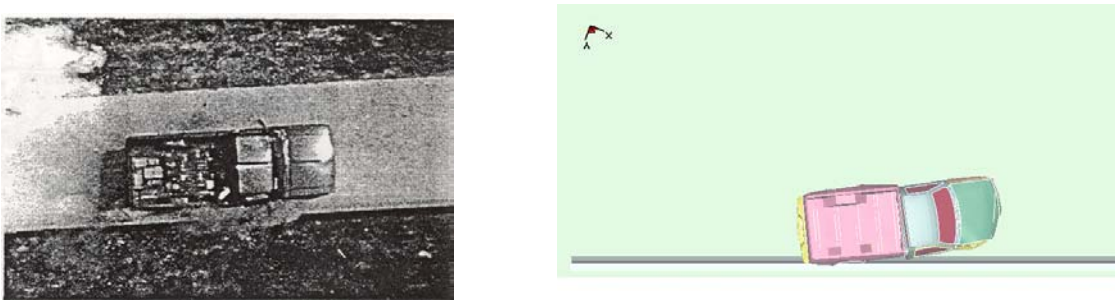

t = 0.250 sec.

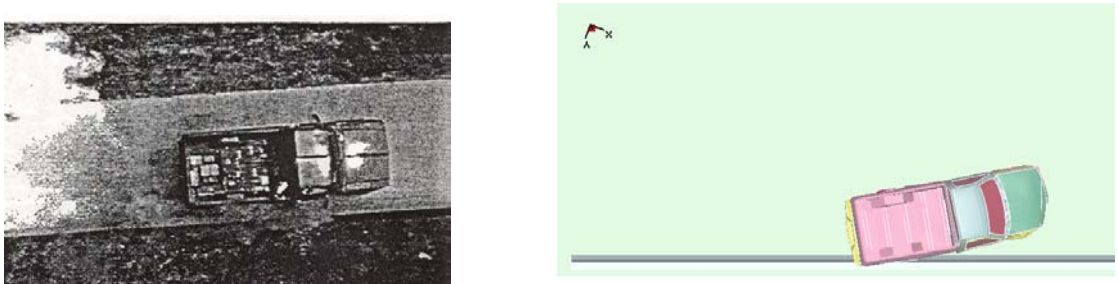

t = 0.308 sec.

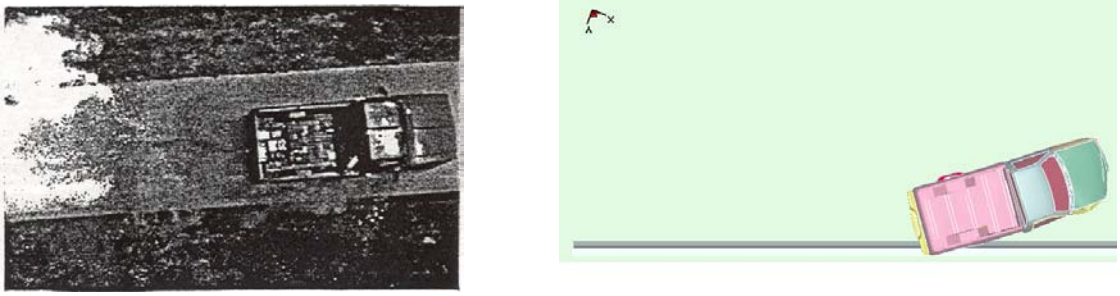

t = 0.376 sec.

Figure 13. Overhead comparison of AASHTO PL-2 full-scale crash and a finite element simulation of an impact with a rigid F-shape bridge railing (continued).

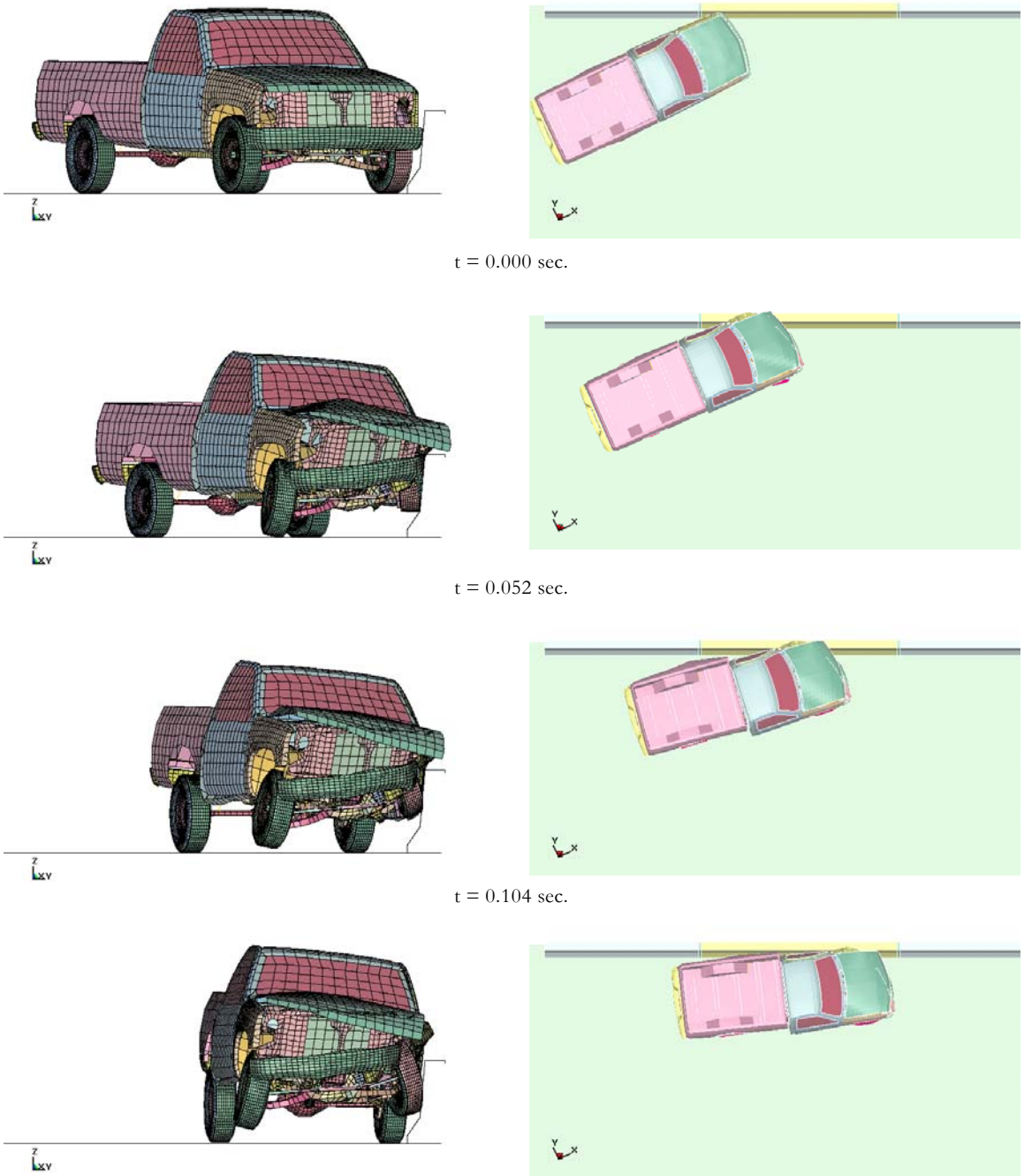

Figure 14. Sequential downstream and overhead views of a finite element simulation of an impact with a rigid F-shape bridge railing under Report 350 Test 3-11 conditions.

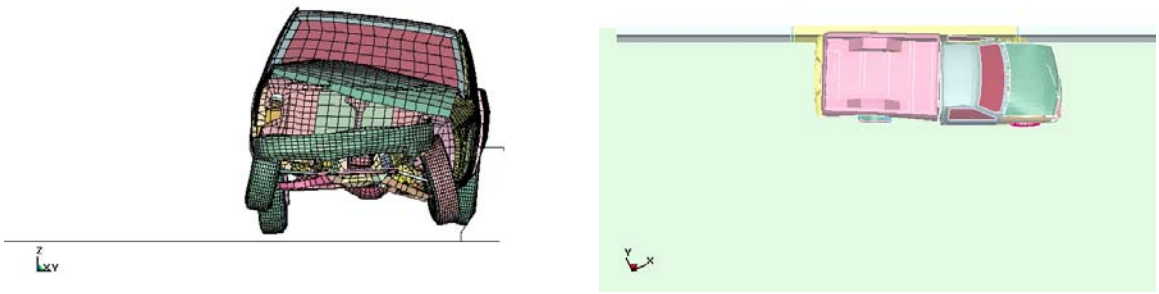

t = 0.208 sec.

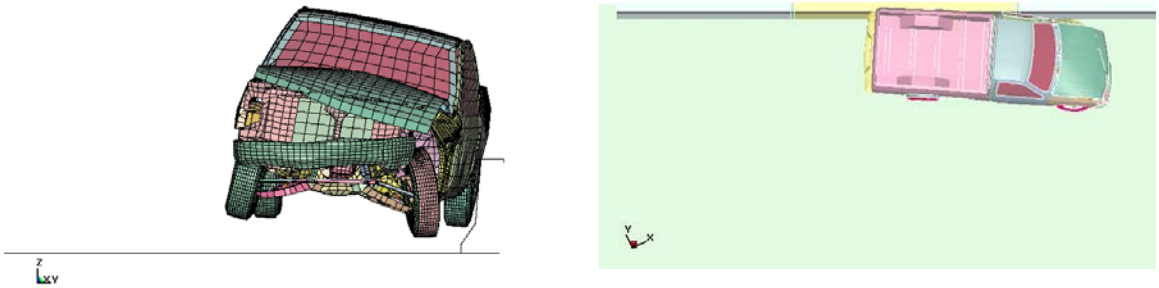

t = 0.260 sec.

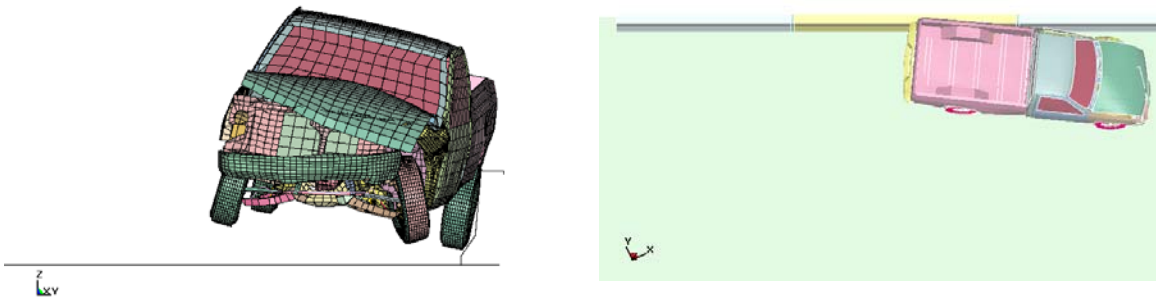

t = 0.300 sec.

Figure 14. Sequential downstream and overhead views of a finite element simulation of an impact with a rigid F-shape bridge railing under Report 350 Test 3-11 conditions (continued).

Next, a finite element simulation of the Test 3-11 was performed. Since the finite element model conservatively predicted the results of the AASHTO PL-2, we can be reasonably confident that the model will likewise conservatively predict the results of an actual crash test of a rigid concrete F-shape were performed. The same C2500 truck and rigid F-shape barrier models were used to performed a finite element simulation corresponding to Report 350 Test 3-11. This simply involved changing the impact conditions from the previous AASHTO PL-2 simulation to conform to the Test 3-11 conditions. The results of this simulation are summarized in Table 2 and Figure 14. Not surprisingly, the finite element simulation predicts that the rigid F-shape barrier would pass the Report 350 test criteria. The quantitative values for the simulation are shown in Table 2 and sequential views of the impact are shown in Figure 14.

In principle, the finite element model of the C2500 pickup truck could be used to simulate an impact using a detailed model of the aluminum parapet and median railings. Unfortunately, the truss-core structure of the aluminum railings makes this impractical because the element size required to capture all the detail of the truss work is very small resulting in a very large model. Instead, the rigid F-shape barrier model discussed in the previous paragraphs was used to capture a time history of the loads at each node on the face of the barrier. This time history was saved in a separate file and then used to apply the same loadings to a very detailed model of each of the aluminum barriers. A much more detailed and complete description of the finite element models and the methods for collecting the load data for this problem can be found in a thesis by Oldani but the procedure is summarized below. [9]

Test Parameter	Simulation	
Test Vehicle		
Type	C2500	
Test Inertial Mass	2008	kg
Impact Conditions		
Velocity	100.0	km/h
Angle	25.0	deg
Exit Conditions		
Velocity	78	km/hr
Angle	5.8	deg
Occupant Impact Velocity (OIV)		
Longitudinal	6.8	m/s
Lateral	9.1	m/s
Occupant Ridedown Acceleration (ORA)		
Longitudinal	5.6	g's
Lateral	8.4	g's
CEN Parameters		
THIV	39.7	km/hr
PHD	10.4	g's
ASI	2.1	
Max. 50 msec average		
Longitudinal	11.6	g's
Lateral	16.6	g's
Vehicle Rotations		
Maximum Roll	13.0	deg
Maximum Pitch	4.1	deg
Maximum Yaw	31.1	deg

Table 2. Results of simulation of Report 350 Test 3-11 conditions for a rigid F-shape barrier.

A layer of shell elements was placed across the face of the barrier to serve as a sensing surface for the loads. These elements were made of null material so they had no stiffness or mass and therefore did not affect the response of either the vehicle or the barrier. The sensing elements were rigidly connected to the barrier and a contact definition was placed on the surface such that the force transmitted by the vehicle to the barrier could be measured at each time step. The sensing surface was 5-m long and included the whole region of the barrier where contact was expected based on past crash testing. The sensing elements were approximately 50 mm square so the load was recorded at 3,434 specific locations on the face of the barrier (i.e., 101 rows in the longitudinal direction and 34 in the vertical direction along the face of the barrier). The resultant load at each of these locations was calculated and saved in an external file at 6.6 μs (i.e., $6.6(10)^{-3}$ msec) intervals such that when the run

was complete, a time history file of the loads at each of these locations was obtained.

Figure 15 shows plots of the lateral (i.e., normal), longitudinal (i.e., tangent) and vertical load time histories resulting from a Test 3-11 impact with a rigid F-shape barrier. As shown in Figure 15, there are two distinct signal signatures; the first shows the primary impact with the vehicle that starts at the time of impact and ends at roughly 120 msec. The second signature corresponds to the back of the pickup truck "slapping" the barrier. This event occurs roughly between 180 and 250 msec. The maximum lateral load observed in the finite element simulation of Test 3-11 during the primary impact event (i.e., up until 120 msec after impact) was 410 kN (i.e., 92 kips) and the average in this range was approximately 300 kN (i.e., 67 kips). The maximum longitudinal and vertical loads during this phase of the collision were both less than 125 kN (i.e., 28 kips) as shown in Figure 15. Figure 16 shows the average heights of the lateral, longitudinal and vertical load resultants above the bridge deck. The average height of the lateral load resultant during the first and phase of the collision was 545 mm and the maximum height was 695 mm, well below the 856-mm (i.e., 33.7 in) height of the barrier.

Interestingly, the AASHTO LRFD Bridge Specification equivalent static loads for Test Level 3 require the use of a 240 kN lateral load applied 685 mm above the bridge deck. The AASHTO equivalent static loads are similar to the values found in the dynamic finite element simulation of the Test Level 3 event; the dynamic load is a little higher but applied at a slightly lower level. This indicates that the AASHTO LRFD procedure for test level three should result in reasonably similar designs to this dynamic analysis.

The second signature in Figures 15 and 16 indicates the impact between the bed of the truck and the barrier. The bed "slapping" the bridge railing toward the end of the event is a shorter duration, lower magnitude impact event. The maximum lateral loading in this second phase of the collision is 213 kN (i.e., 48 kips) and the average is about 125 kN (i.e., 28 kips). The maximum height of lateral load application in the second phase of the collision is 785 mm but the average is a much lower 391 mm as shown in Figure 16.

Once the load at every node on the barrier face was known for every time during the Test 3-11 impact with the rigid F-shape barrier, this time-based load was applied to the face of the aluminum barriers of interest in this project.

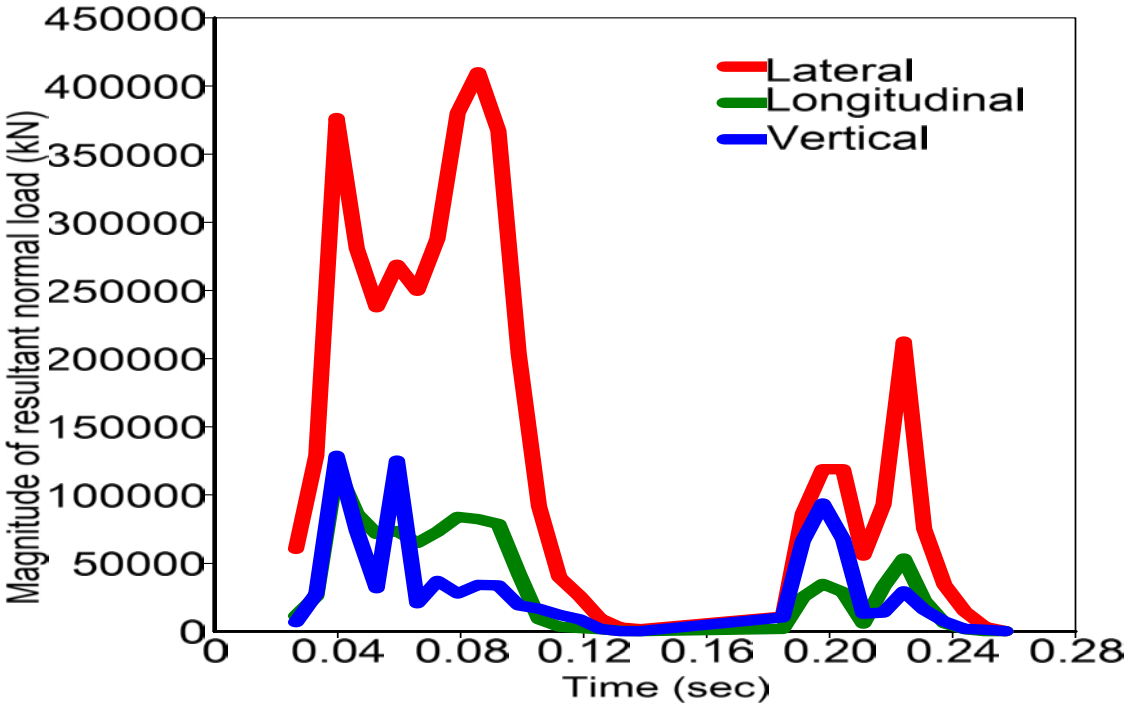

Figure 15. Lateral, longitudinal and vertical contact force resultants as a function of time for a Test 3-11 impact with a rigid F-shape barrier.

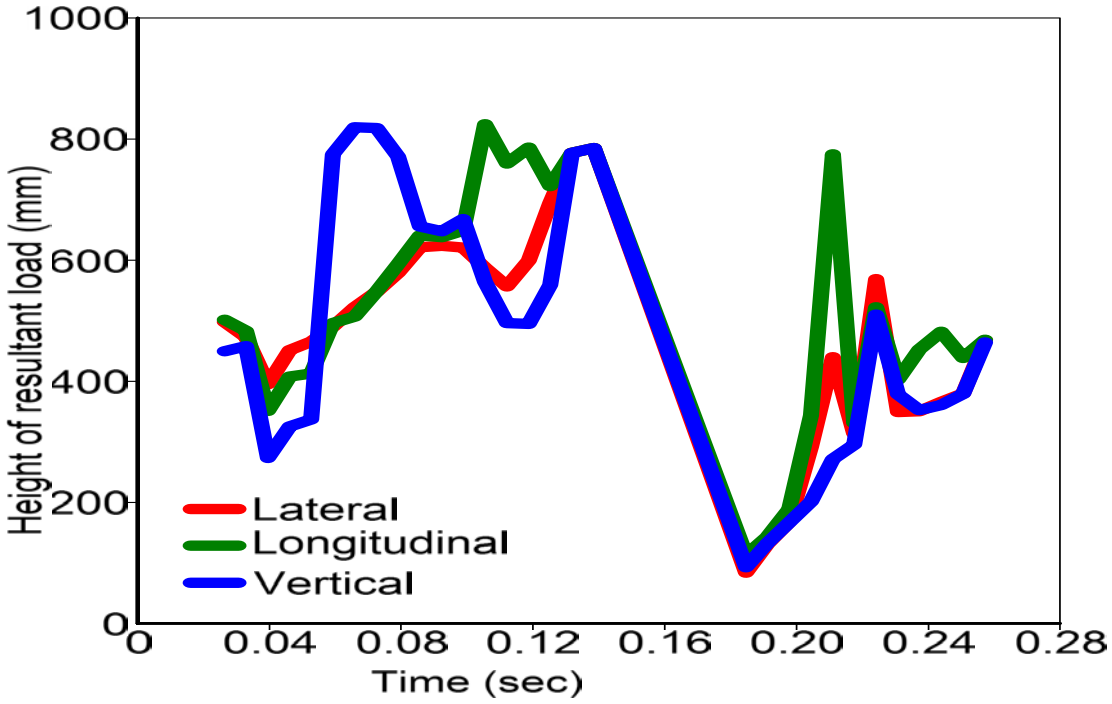

Figure 16. Lateral, longitudinal and vertical height of force resultant as a function of time for a Test 3-11 impact with a rigid F-shape barrier.

Application of dynamic loads to the F-shape parapet bridge railing

As discussed in the previous section, a time history file of the loads at 3,434 specific points on the barrier was obtained by performing a finite element analysis of a Report 350 Test 3-11 of a rigid F-shape bridge railing. These loads were then applied to the finite element model of the aluminum bridge railing and the aluminum median barrier described at the beginning of this paper. Applying this file of loads as a function of position and time to the prospective aluminum barriers is equivalent to performing a finite element simulation or full-scale test of the barrier. The result of such an analysis is the stresses and strains experienced by the two aluminum barrier configurations under Test 3-11 conditions. If the barriers withstand the application of the forces with acceptable stresses and only small localized permanent deflections, the barriers can be judged to satisfy the test level three conditions.

A detailed finite element model of the aluminum F-shape bridge parapet railing, shown earlier in Figures 2 and 8, was developed. Because the truss work in the panels is very thin, a very detailed model containing over 600,000 elements (579,950 of which were solid elements used to represent the intricate extruded aluminum truss core panels and top rails) with very small elements was necessary. A 0.5 μs time step was required due to the small element size and the total simulation time was 317 msec. A much more detailed and complete description of the finite element models and the methods for collecting the load data for this problem can be found in a thesis by Oldani.[9]

The results of the application of the Test 3-11 loads are summarized in Figures 17 through 20. There were only local plastic deformations of the post near the front edge of the weld. These localized stresses, shown as red spots in Figure 17, were above the yield stress for 6061-T6 aluminum but still well below the failure limit. The maximum loading occurred at the first post downstream of the impact at about 60 msec after the impact. The compression flange of the post, a region where the analysis had uncovered buckling problems with earlier versions of the post, experienced stress well under the yield stress at the maximum post loading. There were also some localized permanent deformations of the face of the truss-core panels where the front bumper and wheel rims contacted the barrier. All of the interlocked connections remained intact and showed no tendency to pull apart during the impact. Likewise the bolted connections and clamp bars remained in the elastic region even at the time of maximum loading.

The global lateral deflections of the barrier measured at several points at the very top of the bridge railing were obtained and a time history is shown in Figure 18. The maximum dynamic lateral loading occurred roughly at the midspan and was a modest 37 mm. There was a significant spring-back effect such that the final maximum permanent deflection at the top of the barrier was only 5 mm. The reason for this is that there is very little plastic deformation anywhere in the barrier so most of the strain energy is returned elastically after the maximum loading has passed.

Figure 19 shows a total energy balance and Figure 20 shows an energy balance for the major components of the bridge railing. A comparison of the data in the two figures shows that the upper truss-core panel absorbs about 30 percent of the strain energy and the top rail absorbs about 15 percent of the strain energy at the peak loading. The lower truss-core panel, the post web, the post flanges and the toe clips are responsible for the remaining strain energy absorption in roughly equal amounts. About 65 percent of the total strain energy remains elastic explaining the very small lateral deflections. The remaining 35 percent of total strain energy is accounted for by a variety of localized deformations in the face of the barrier and the base of the post as described earlier.

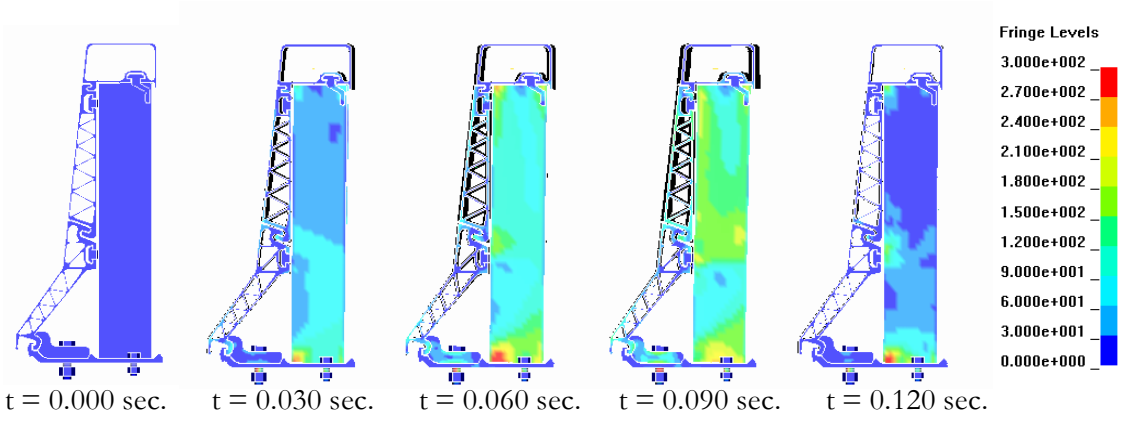

Figure 17. Von Misses stress contours of the aluminum bridge parapet under Report 350 Test 3-11 conditions.

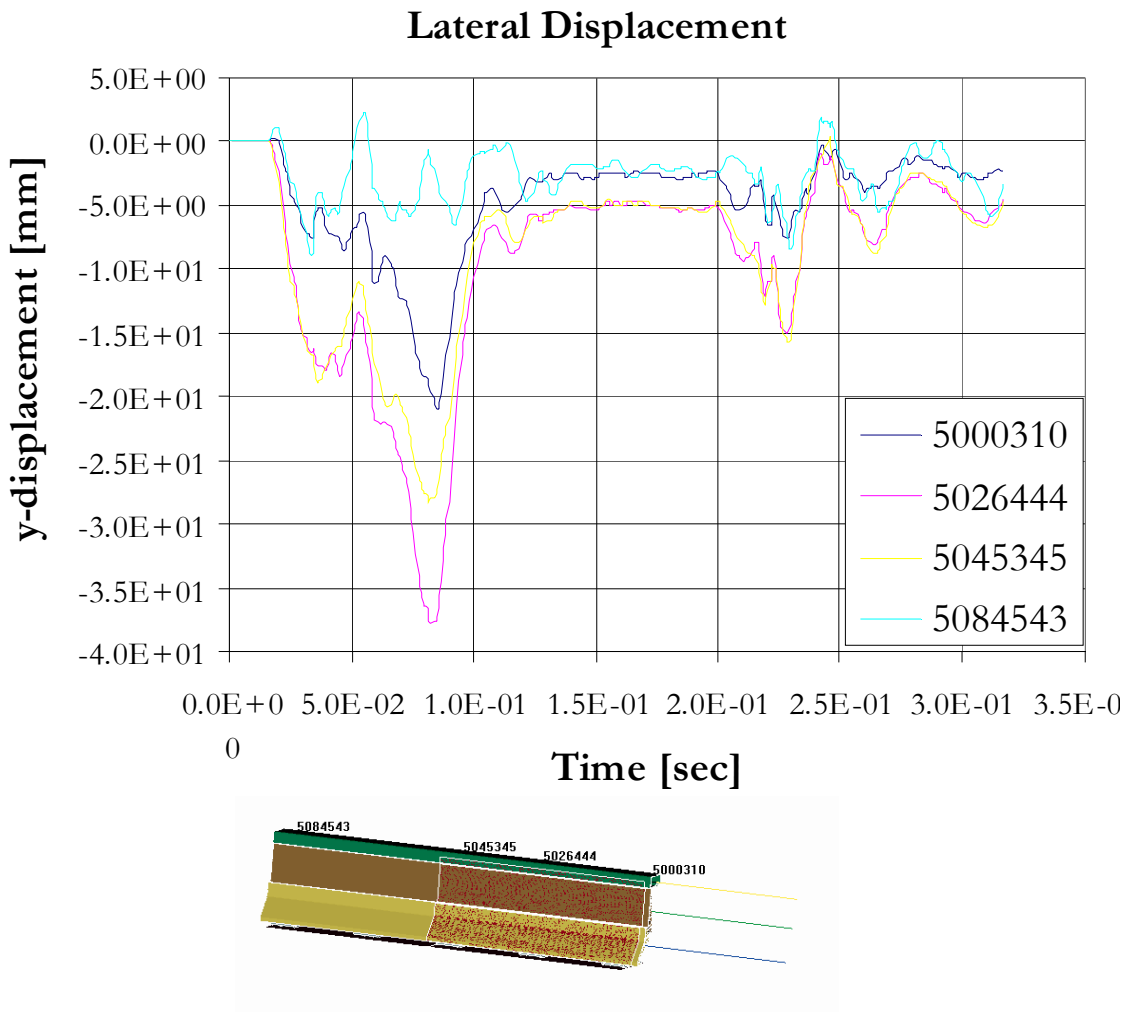

Figure 18. Lateral displacement of the top of the aluminum bridge parapet under Report 350 Test 3-11 conditions.

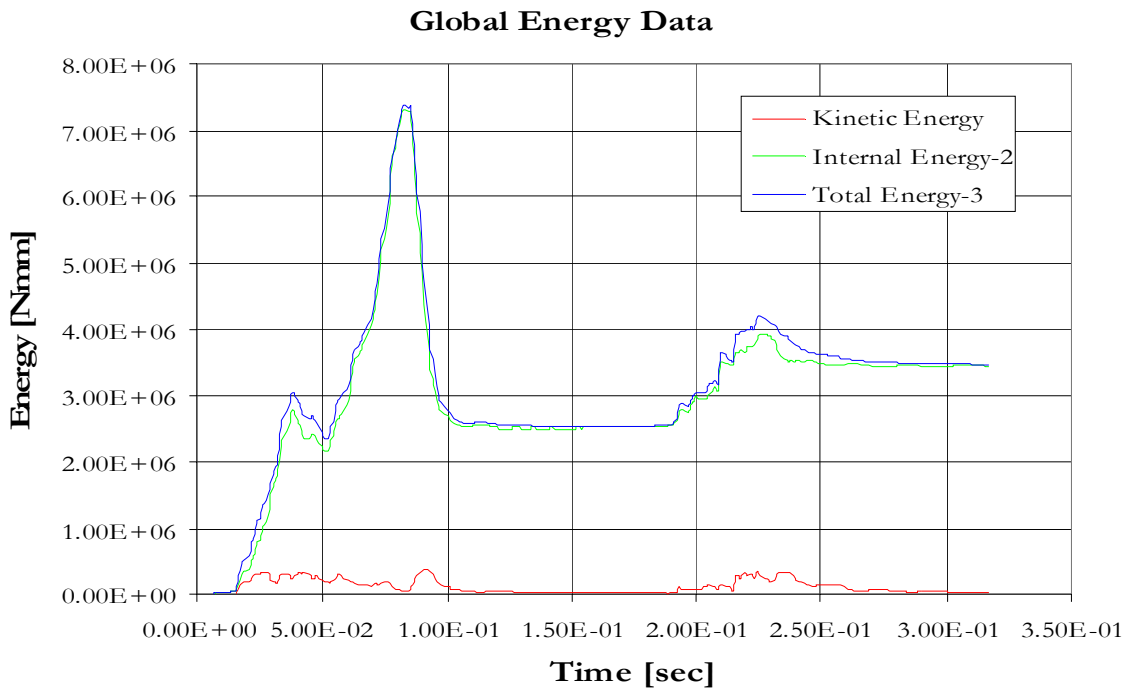

Figure 19. Total energy balance for the aluminum bridge parapet under Report 350 Test 3-11 conditions.

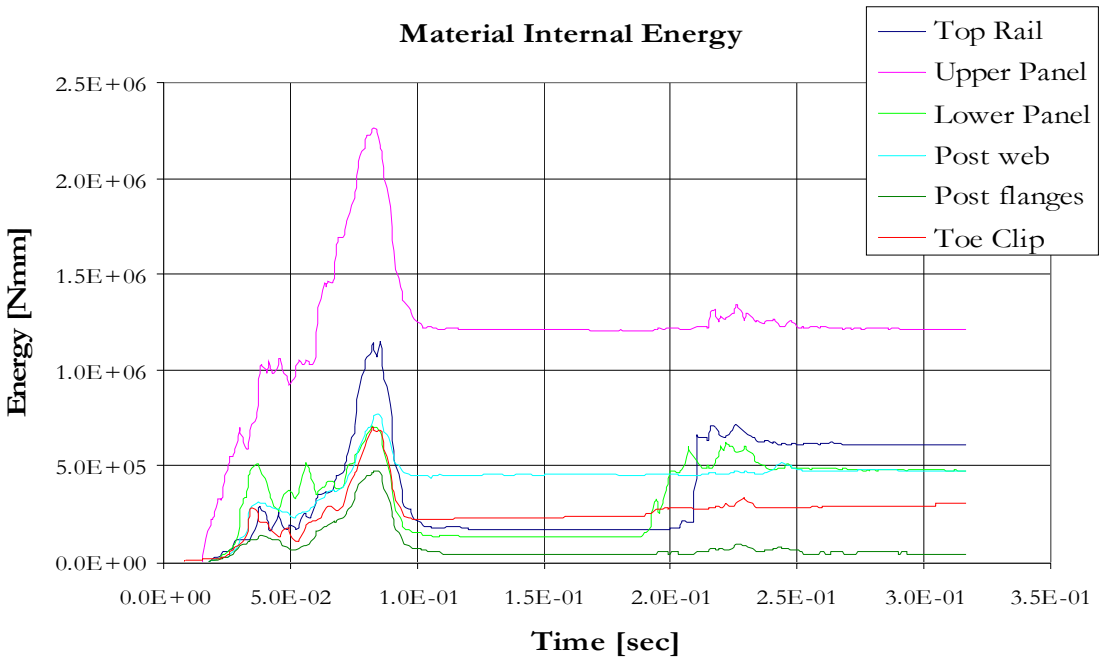

Figure 20. Energy balance for the components of the aluminum bridge parapet under Report 350 Test 3-11 conditions.

Since only minor localized deformations occurred and the barrier retained its structural integrity throughout the impact event, the aluminum parapet bridge railing is essentially rigid. A maximum dynamic deflection of 37 mm and a permanent lateral deflection of 5 mm is very small considering the geometry of the railing and the severity of the impact. Since the aluminum parapet bridge railing performs as an essentially rigid barrier, it can be presumed that a full-scale crash test of this barrier would result in essentially the same responses as a full-scale test with a concrete barrier rigidly attached to the bridge deck. Since a concrete F-shape barrier is already presumed to satisfy the test level three criteria it can be inferred that the aluminum parapet bridge railing also satisfies Report 350 test level three.

Application of dynamic loads to the median barrier

In similar fashion an analysis was performed of the aluminum median barrier. A detailed finite element model of the aluminum F-shape median barrier, shown earlier in Figure 8, was developed and a finite element simulation was performed using the load time-history file representing a Test 3-11 collision.

Stress contours at various times in the impact are shown in Figure 21 for the barrier face and in Figure 22 for the posts and shear beams. The yield stress for 6063-T6 aluminum, the material for the upper and lower truss-core panels and the top rail, is 172 MPa. As shown in Figure 22, there are some localized regions where contact with the wheel rim and vehicle bumper caused permanent deformations but these deformations are all minor and localized and did not affect the integrity of the panels. The yield stress for 6061-T6 aluminum, the material used for the posts and shear beams, is 241 MPa. As shown in Figure 22, there are some small regions of plastic flow at the base of the posts near the welds. The stresses are about 300 MPa, greater than the yield stress but still well below the failure limit. Deformations of the median barrier, therefore, are generally elastic with only a few minor localized plastic deformations.

The lateral deflection of the barrier is summarized in Figure 23. The maximum dynamic lateral deflection occurred approximately at the midspan and had a value of almost 40 mm. Since most of the strain energy is elastic, the permanent deflection was only about 2 mm as shown in Figure 24. For all purposes the barrier behaved in an essentially rigid manner since these are very small deflections.

Figure 24 and 25 show the global energy balance and the energy balance for the major components. Like the bridge parapet version, the majority of the strain energy is absorbed by elastic deformations of the upper truss-core panel and the top rail. In the case of the median barrier, 26 percent of the strain energy is absorbed by the upper truss-core panel and 10 percent is absorbed by the top rail. The remaining 64 percent of the strain energy is roughly equally divided among the other major components, each accounting for approximately 10 percent of the total. As shown in Figure 24, half the strain energy is returned to the structure elastically and the other half represents the permanent localized plastic deformations.

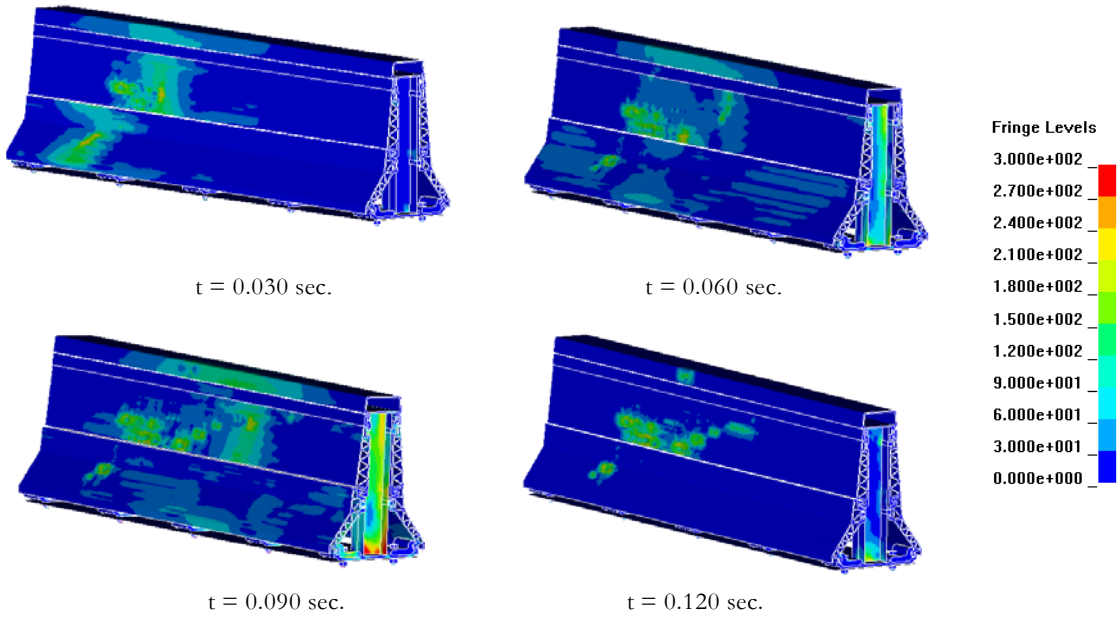

Figure 21. Von Misses stress contours on the barrier face for an aluminum median barrier in Test 3-11 conditions.

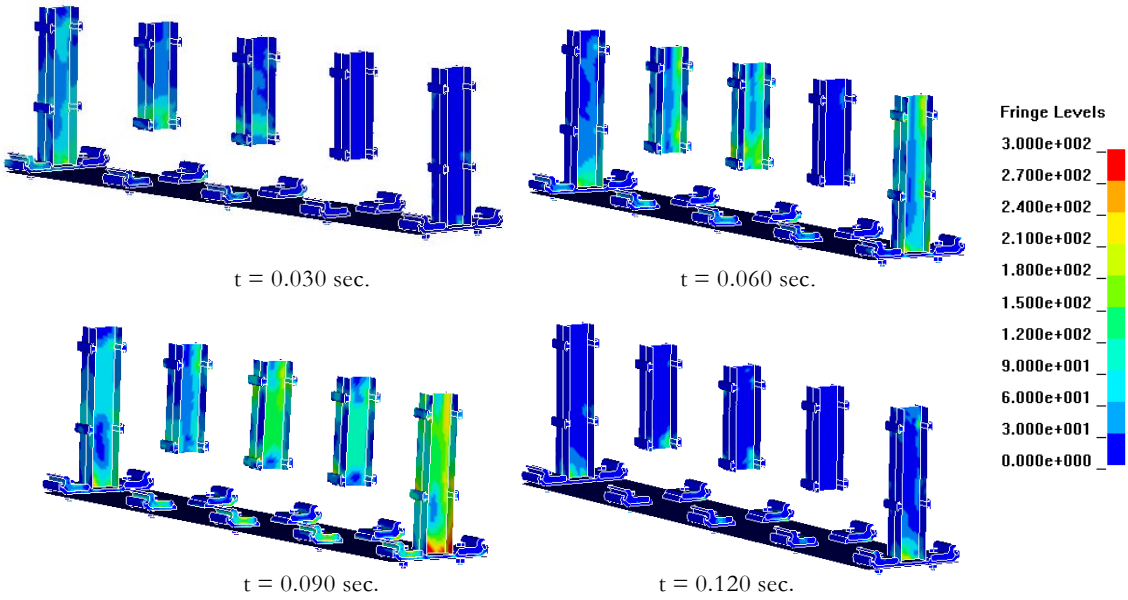

Figure 22. Von Misses stress contours on the posts and shear beams for an aluminum median barrier in Test 3-11 conditions.

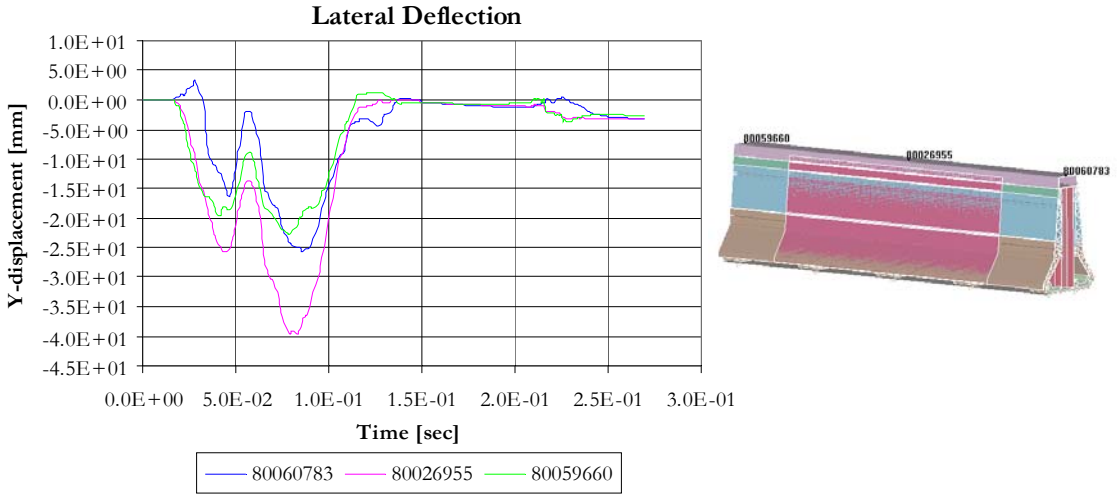

Figure 23. Lateral deflection at the top of the barrier for an aluminum median barrier in Test 3-11 conditions.

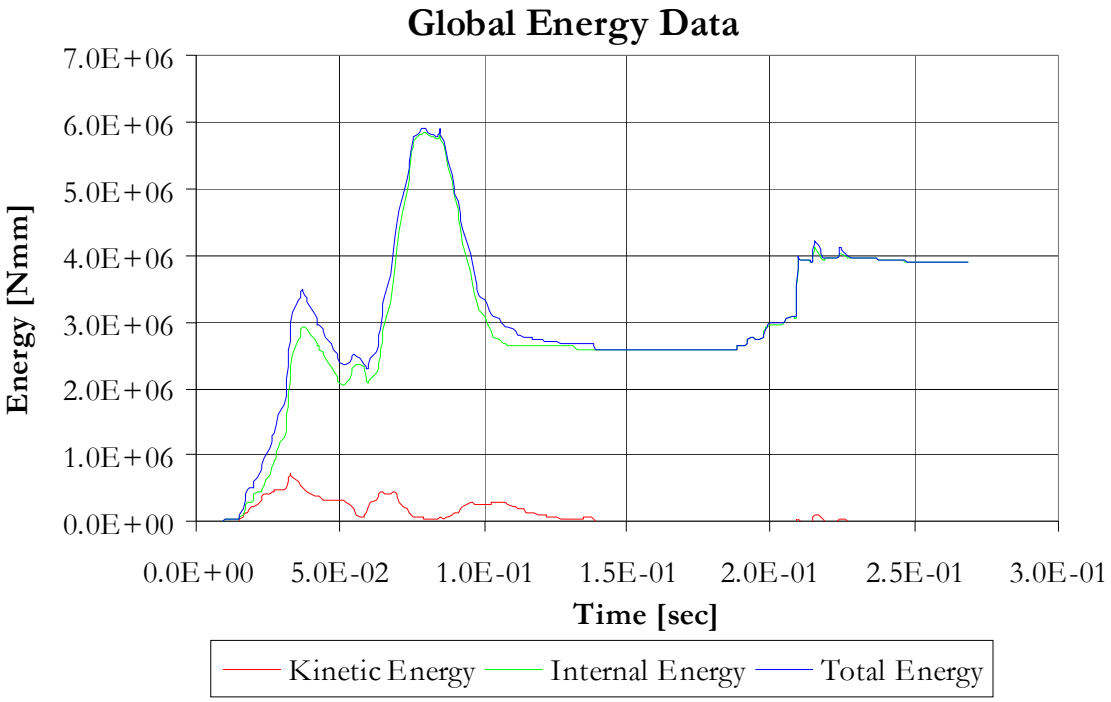

Figure 24. Global energy balance for an aluminum median barrier in Test 3-11 conditions.

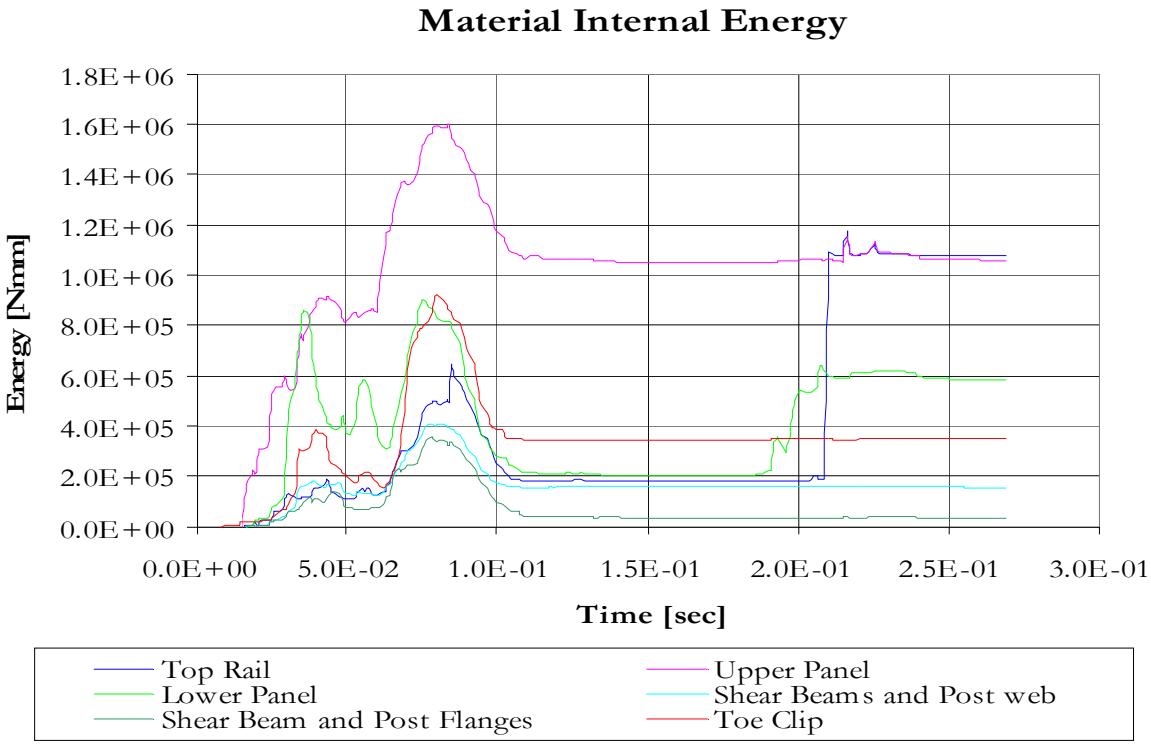

Figure 25. Energy balance for the major components of an aluminum median barrier in Test 3-11 conditions.

Since only minor localized deformations occurred and the barrier retained its structural integrity throughout the impact event, the aluminum median barrier is essentially rigid. A maximum dynamic deflection of 40 mm and a permanent lateral deflection of 2 mm is very small considering the geometry of the railing and the severity of the impact. Since the aluminum median barrier performs as an essentially rigid barrier, it can be presumed that a full-scale crash test of this barrier would result in essentially the same responses as a full-scale test with a concrete median barrier rigidly attached to the bridge deck. Since a concrete F-shape barrier is already presumed to satisfy the test level three criteria it can be inferred that the aluminum parapet bridge railing also satisfies Report 350 test level three.

Static LRFD Analysis for Test Levels Three and Four

Background

In principle a dynamic finite element simulation of a test level four impact between the two aluminum barriers could also be performed using exactly the same models discussed in the previous section. The 8000S vehicle available from the National Crash Analysis Center is still in development phase. The "bullet" model posted on their website is actually a Beta version that has not been validated and is known to have numerous problems. Battelle and Oak Ridge National Laboratory (ORNL) were recently contracted to assess the fidelity of the model for use in NCHRP Report 350 Test Level 4 impact simulations. Simulations of various full-scale tests of test level four impacts into rigid barriers were conducted independently by the two organizations. Their analyses identified several areas of concern in the model that were leading to erroneous results. Battelle, ORNL and the NCAC are currently in the process of enhancing the model for use in test level four impact simulations but the next release of the vehicle model is not expected to be available until late in the summer of 2004.

As an alternative, the AASHTO LRFD analysis procedure was used to evaluate the two barrier designs for test level four. If a rigid barrier (i.e., bridge railing) with the same basic shape as the untested barrier has been tested, all that must be done is to demonstrate that the untested barrier is at least as strong as the crash-tested barrier.[6] The AASHTO Bridge Specification provides a Load and Resistance Factor Design (LRFD) procedure for designing traffic railings.[4] Resistance factors for various barrier components can be found in Table 3.4.1-1 in the AASHTO LRFD Bridge Specification.[4] The resistance factor for vehicle collision events (CT) in the extreme event II category is given as 1.0. Table A13.2-1 provides three specific design loadings that must be used in analyzing a barrier for Report 350 test level 3 and 4 as required by AASHTO LRFD Table A13.2-1. These are summarized in Table 4.

Property	Transverse	Longitudinal	Vertical
TEST LEVEL 3			
Load (kN)	240	80	20
Length (mm)	1220	1220	5500
Distributed Load (kN/m)	200	65	5
Height of Application (mm)	685	685	top
TEST LEVEL 4			
Load (kN)	240	80	80
Length (mm)	1070	1070	5500
Distributed Load (kN/m)	225	75	15
Height of Application (mm)	810	810	top

Table 4. Equivalent Static Loads for Test Levels 3 and 4 based on the AASHTO LRFD Bridge Specification.

In principle for a system like the aluminum bridge railing with posts and beam elements there are six load cases required by the AASHTO LRFD specification for each test level:

- Transverse loads
  - Centered on the post and
  - Centered on the mid-span.
- Longitudinal loads
  - Centered on the post and
  - Centered on the mid-span.
- Vertical loads
  - Centered on the post and
  - Centered on the mid-span.

Performing the analysis for both the parapet and median barrier railings for both tests would, therefore, involve 24 separate analyses. Fortunately, many of these analyses are not really necessary and can be eliminated. For example, if a barrier passes the test level four analyses there is no point in performing the test level three analyses since the test level three loading is a lower intensity distributed load applied at a lower height. This reduces the total number of tests to six per barrier.

Both transverse loading tests for test level four are necessary since the transverse load may fail the post or its connection to the deck (i.e., the loading centered on the post) or the truss-core panels in bending (i.e., the loading centered on the midspan). These two tests are probably the two most important tests in the group. The longitudinal load arises primarily from vehicle-barrier friction and potential vehicle-barrier snagging. The aluminum barriers have a smooth face so snagging between the vehicle and barrier is very unlikely and friction between the barriers is small since it involves metal to metal contact. An analysis of the longitudinal loads is not needed. The vertical loads represent the cargo deck of a truck striking the top of the barrier. Barriers like the aluminum bridge parapet and median barrier that include short posts will be very strong if struck from above directly on the post. The vertical load centered on the midspan is a more revealing test of the barrier since the top rail and truss core panels need to transfer the load in bending to the posts and deck.

The median barrier design is much stiffer than the bridge parapet design as shown in the dynamic analysis section presented above. The same truss core panels are used with similar post and base plate connections to the deck. The median barrier has truss core panels on both sides which add considerable stiffness to the system. Since the median barrier design is so much stiffer than the bridge parapet, it would appear that if the aluminum F-shape bridge parapet performs satisfactorily then the median barrier must also perform well. The adequacy of both designs can, therefore, be assessed by evaluating the following three load cases on the aluminum F-shape bridge parapet design:

- A transverse load centered on the post,
- A transverse load centered on the mid-span, and
- A vertical load centered on the mid-span.

The AASHTO LRFD Bridge Specification provides analysis procedures for simple barrier types like concrete parapet railings and post-and-beam type railings. Unfortunately, the aluminum parapet bridge railing and the aluminum F-shape median barrier are complex structures that involve complicated geometry and extruded truss-core panels that do not lend themselves to simple hand analysis methods.

The aluminum barriers are highly indeterminant (this is beneficial since it provides more load paths but it makes the analysis more complicated) so a non-linear quasi-static finite element analysis using the loads required by the AASHTO LRFD Bridge Specification is the only possible method for assessing the adequacy of these two railings by the AASHTO LRFD procedure. The results of the quasi-static analyses for test level four are presented in the following sections. The analyses were performed using LS-DYNA where the loads shown in Table 4 were applied quasi-statically to the same barrier models discussed earlier in the report.

Application of quasi-static loads to the F-shape parapet bridge railing

240 kN transverse load centered on a middle post

The first load case involves a 240 kN load applied vertically across the face of the top rail at a height of 810 mm above the bridge deck. The load was applied centered on a middle post and extended longitudinally 535 on each side of the post. This loading provides a critical test of the strength of the post, baseplate and front bolts. Figure 26 shows a cross-section view through the post at the point of maximum deflection and Figures 28 and 29 show closer views of the effective stresses around the connections. The maximum deflection at the height of load application (i.e., 810 mm) was 48 mm. The maximum stresses in the post, as shown in Figures 26 through 29, were located on the tension side of the web above the point where the upper and lower truss core panels are connected. The maximum post stress was 317 MPa, close to the failure stress of the material. While the stresses were approaching high levels, the deflection was still quite moderate, the deformations were very localized and the barrier system still maintained its integrity. As shown in Figure 28 and 29, the tongue-and-groove connections between the lower and upper truss core panels and the upper truss core panel and the top rail all maintained their integrity and did not pull open. The stresses in these connections generally remained less than the yield stress of the 6063-T6 aluminum material. There were several very small regions of near-failure stress due to contact stresses in the connection between the upper and lower truss core panels but these represent very localized stresses represented by the small yellow and red spots in Figure 29. The base plate experienced high bending stresses on a section through the bolt hole as shown in Figure 27. The maximum stress in the base plate was 275 MPa, high but only slightly above the 241 MPa yield stress of the material and still well below the 317 MPa failure stress of the material. The net tensile force on each of the 24-mm diameter front bolts was 290 kN, just below the 293 kN minimum tensile strength of an M24 A325 bolt. The results of this quasi-static analysis of the AASHTO LRFD transverse loading for test level four indicate that the bridge railing has sufficient strength to successfully redirect the 8000S truck in a Report 350 TL-4 impact.

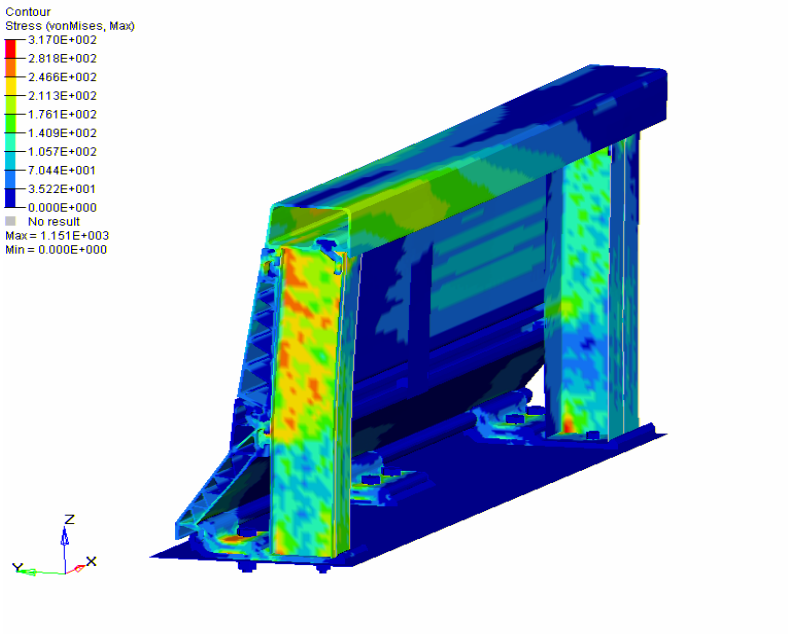

Figure 26. Effective stress contour and section cut at the point of maximum deflection for the AASHTO LRFD transverse centered-on-post test level four load case.

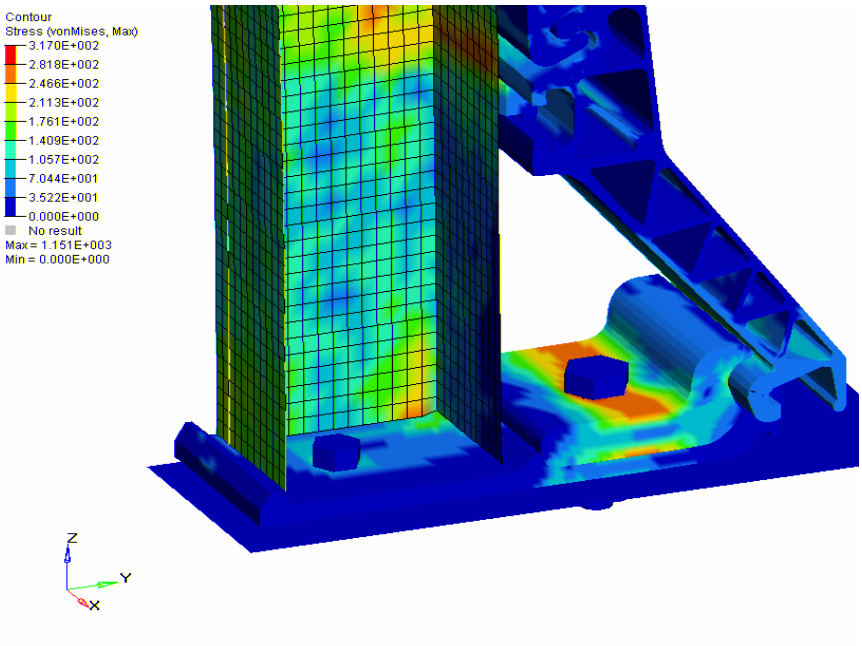

Figure 27. Effective stress contours on the lower post and base plate at the point of maximum deflection for the AASHTO LRFD transverse centered-on-post test level four load case.

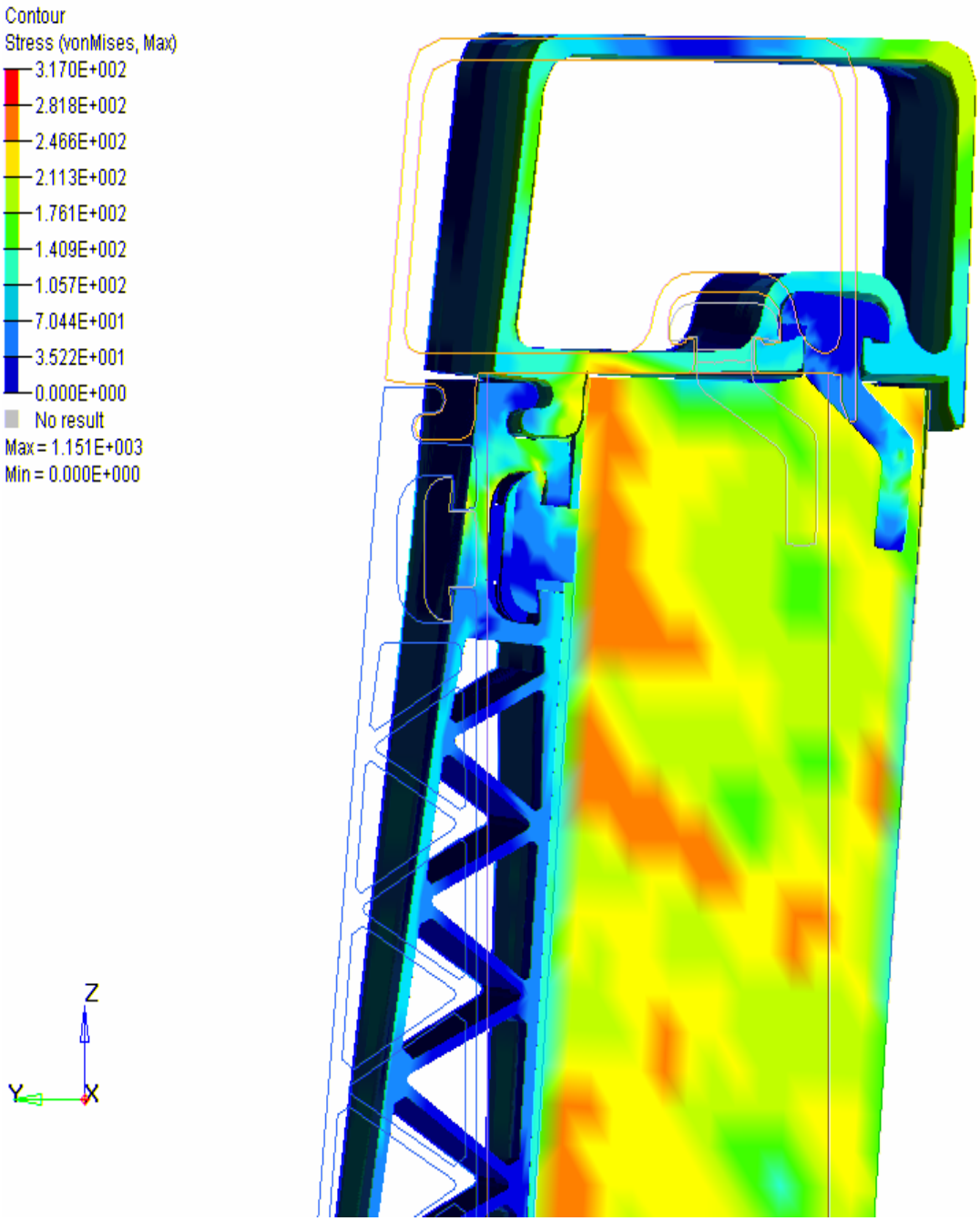

Figure 28. Effective stress contours on the upper section of the barrier at the point of maximum deflection for the AASHTO LRFD transverse centered-on-post test level four load case.

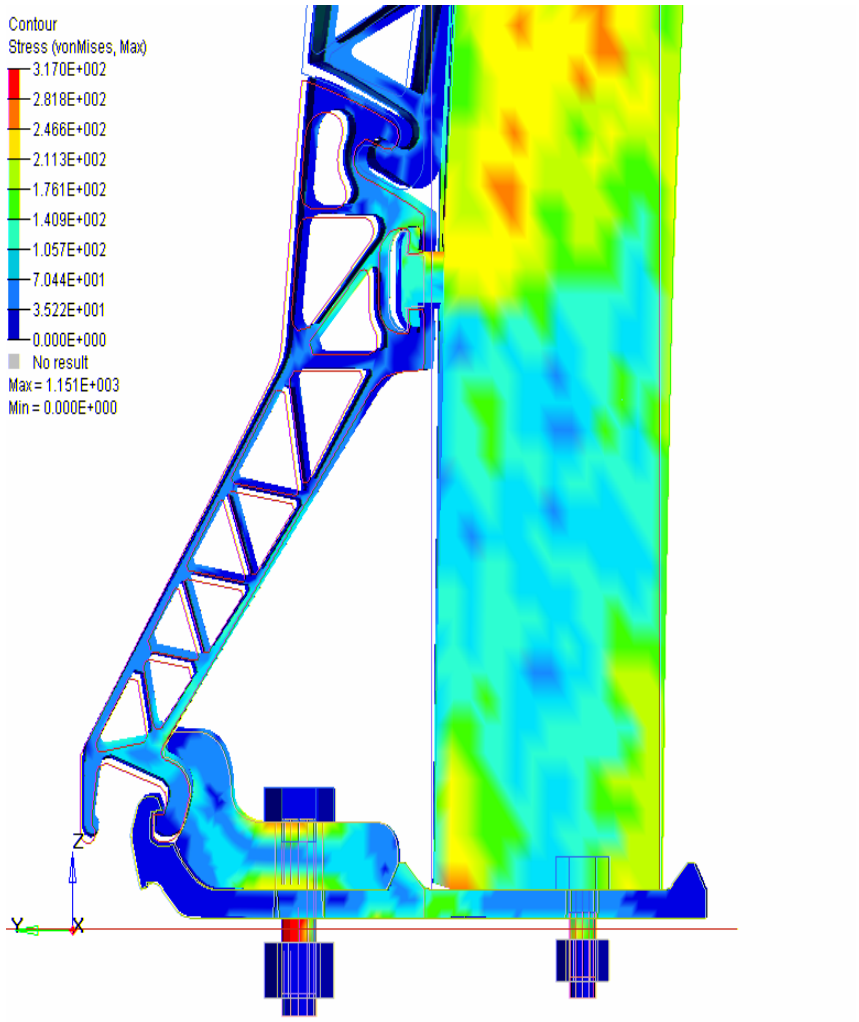

Figure 29. Effective stress contours on the lower section of the barrier at the point of maximum deflection for the AASHTO LRFD transverse centered-on-post test level four load case.

240 kN transverse load centered on the midspan

The second load case involves a 240 kN load applied vertically across the face of the top rail at a height of 810 mm above the bridge deck. The load was applied centered on the midspan point between two middle posts and extended longitudinally 535 on each side of the mid-span point. This loading provides a critical test of the strength of the upper and lower truss core panels and the top rail. Figure 30 shows a cross-section view through the post at the point of maximum deflection and Figures 31 and 32 show closer views of the effective stresses around the connections. The maximum values of the effective stress contours in Figures 30 through 32 are set to the failure stress of the aluminum material, 317 MPa. There were two points of high stress concentration in the posts as shown in Figure 30: one at the base of the web at the front of the post and the other in the flange just above the connection point of the front panel to the post at approximately 310 mm above the base. These post stresses were high but below the failure stress of 317 MPa. The maximum effective stress in the upper toe clip of the bolted base plate was less than 140 MPa at the post location as shown in Figure 31. There were some higher stress concentrations at the mid-span toe clip locations but aside from these local concentrations the stresses were also generally below 140 MPa at the midspan toe clip as well, as is also shown in Figure 31. The maximum deflection at the height of load application (i.e., 810 mm) was 42 mm and this occurred at the mid-span. The maximum stress in the truss core panels was approximately 255 MPa as shown in Figure 32, just slightly above the yield stress. The stresses are relatively low in the truss core panels because of the way they are attached to the rest of the system and the point of loading. The load is applied to the top rail, but the connection of the top rail to the truss core panels is not much more than friction at any point between posts. When load is applied to the top rail, the top rail has to transfer the load to the post and then the post transfers the load back to the truss core panels through the bolted connections. The net tensile force on each of the 24-mm diameter front bolts was 171 kN, well under the 293 kN minimum tensile strength of an M24 A325 bolt. The results of this quasi-static analysis of the AASHTO LRFD transverse loading for test level four indicate that the bridge railing has sufficient strength to successfully redirect the 8000S truck in a Report 350 TL-4 impact.

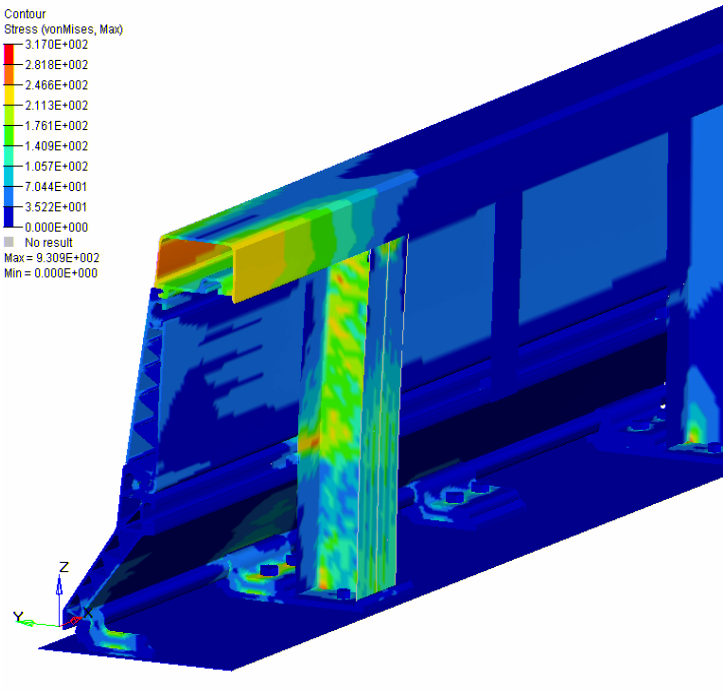

Figure 30. Effective stress contour and section cut at the point of maximum deflection for the AASHTO LRFD transverse centered-on-midspan test level four load case.

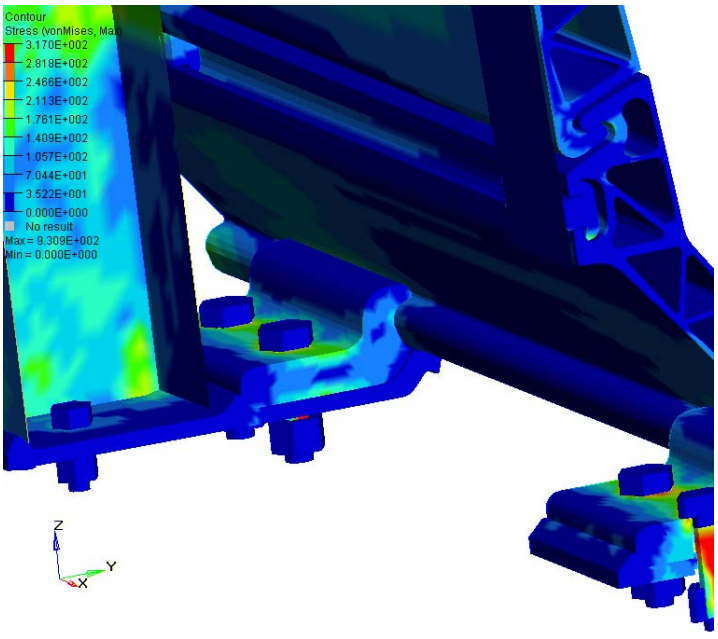

Figure 31. Effective stress contour and section cut at the point of maximum deflection for the AASHTO LRFD transverse centered-on-mid-span test level four load case.

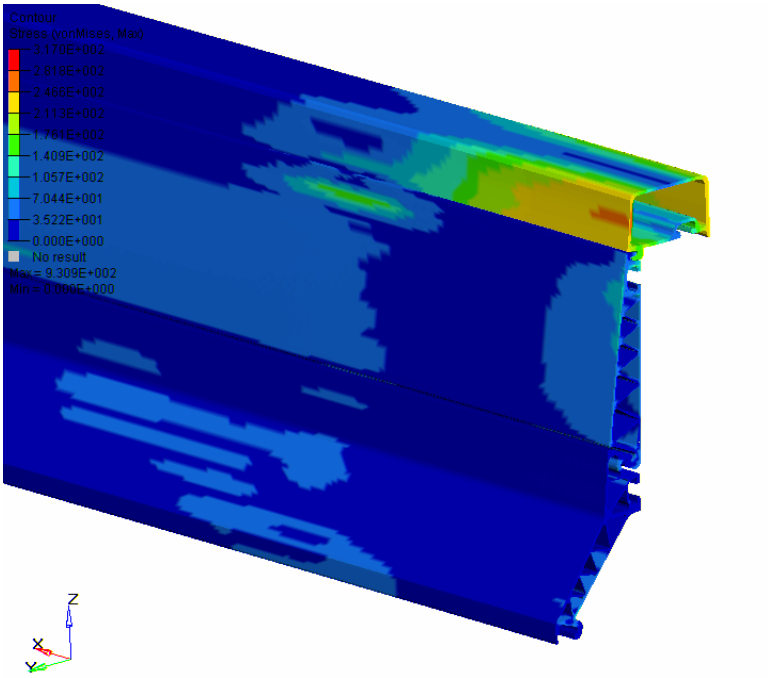

Figure 32. Effective stress contours and at a cut through the truss core panels and top rail at the point of maximum deflection for the AASHTO LRFD transverse centered-on-mid-span test level four load case.

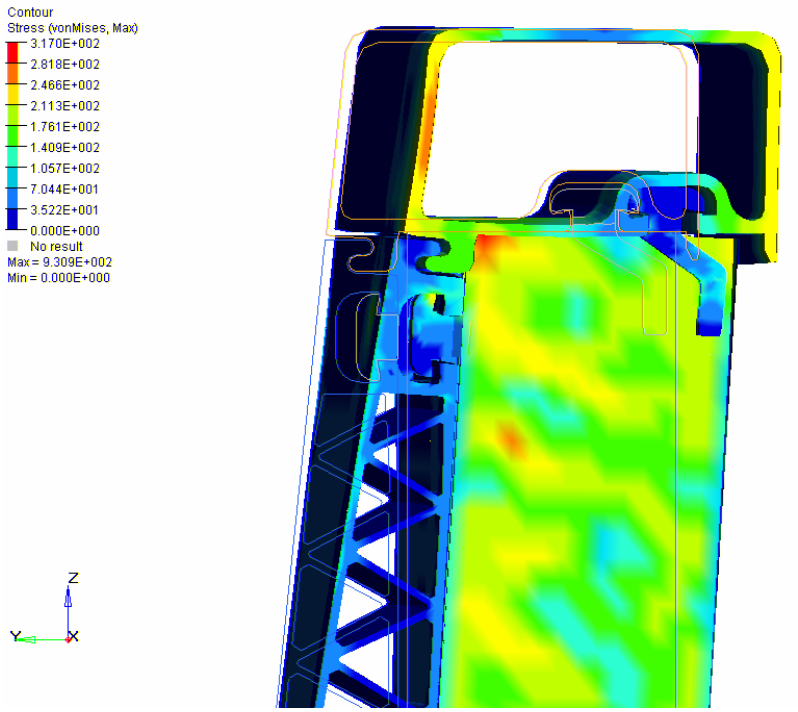

Figure 33. Effective stress contours and at a cut through the post location for the AASHTO LRFD transverse centered-on-midspan test level four load case -- upper portion.

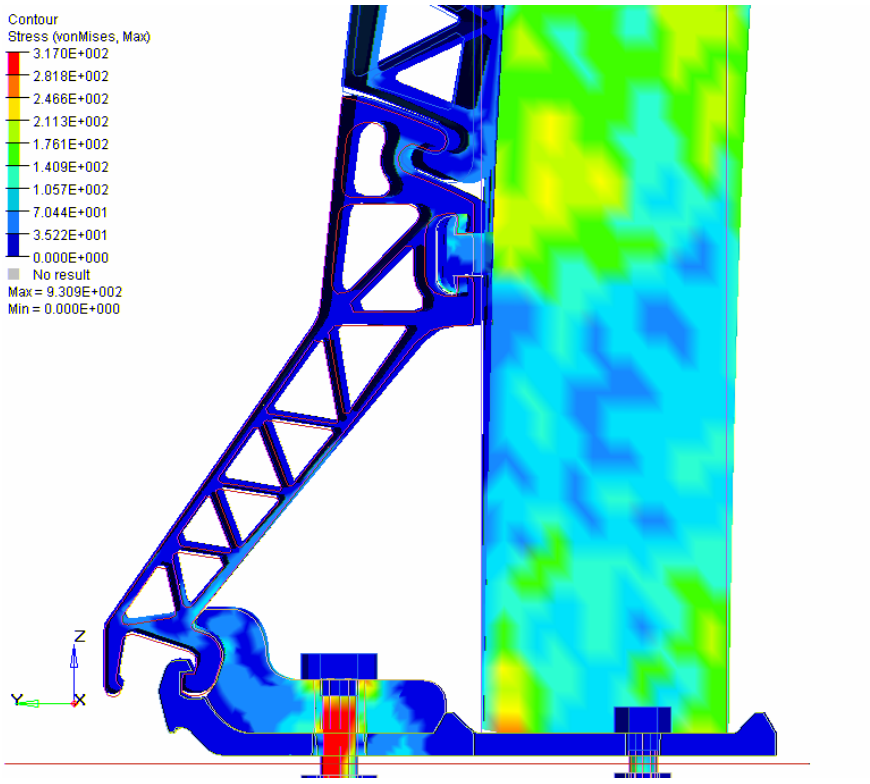

Figure 34. Effective stress contours and at a cut through the post location for the AASHTO LRFD transverse centered-on-mid-span test level four load case -- lower portion.

80 kN vertical load centered on midspan

The third load case involves an 80 kN vertical load applied across the top face of the top rail. The load was applied centered on the mid-span point to maximize the chance of bending the top rail and truss-core panels. The load extends 2775 mm on each side of the mid-span point. This loading provides a critical test of the bending strength of the top rail if the cargo deck of a truck should strike the top of the barrier. The maximum vertical deflection of the top rail at the point of load application (i.e., the mid-span) was 13.4 mm. Figure 35 shows the effective stress along the top rail, the maximum value being just over the yield stress. A cross-section view through one of the adjacent posts is shown in Figure 36. The stresses in the post are quite low with the exception of the area at the bottom front of the flange where they slightly exceed the yield stress. Figures 37 and 38 show cross-sections and stress contours at the mid-span; Figure 37 shows the whole cross-section whereas Figure 38 shows the upper section highlighting the local deformations of the top rail. As shown in Figure 38, the top rail does experience some minor localized deformations but in general the stress, strains and deformations are very low throughout the barrier system under this loading condition. The results of this quasi-static analysis of the AASHTO LRFD vertical loading for test level four indicates that the bridge railing has sufficient strength to successfully sustain a vertical impact with the cargo deck of an 8000S truck in a Report 350 TL-4 impact.

The foregoing quasi-static analyses show that the aluminum F-shape parapet bridge railing has sufficient strength to meet the requirements of the AASHTO LRFD Specification for TL-4 conditions.

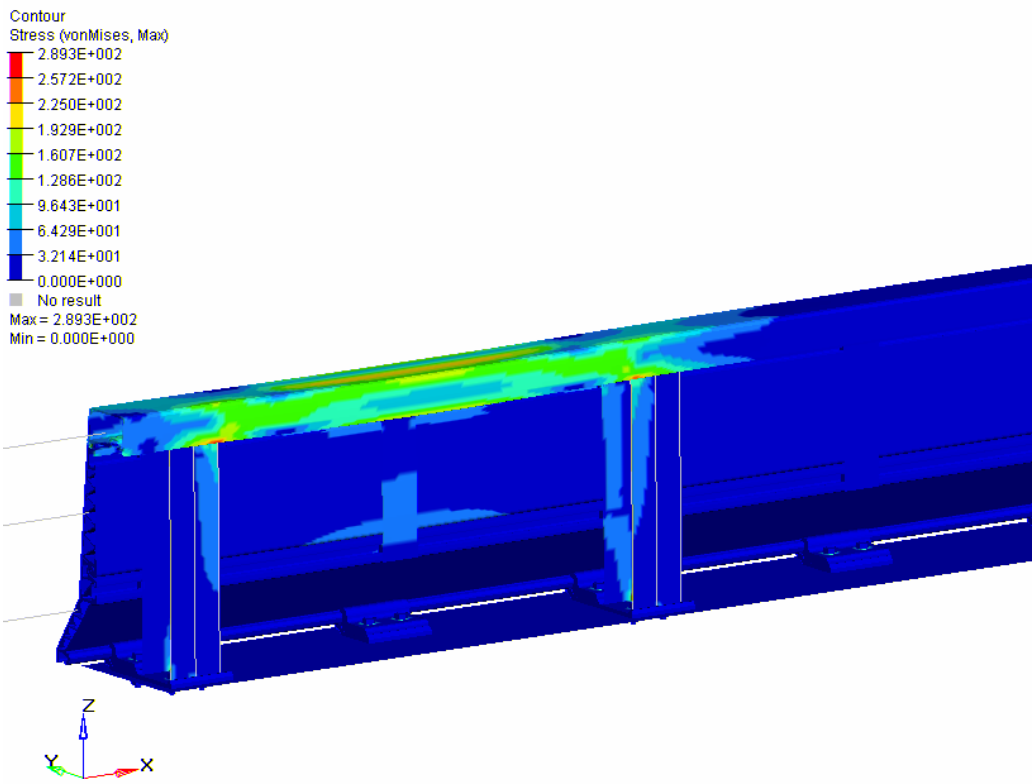

Figure 35. Effective stress contours for the AASHTO LRFD vertical centered-on-mid-span test level four load case.

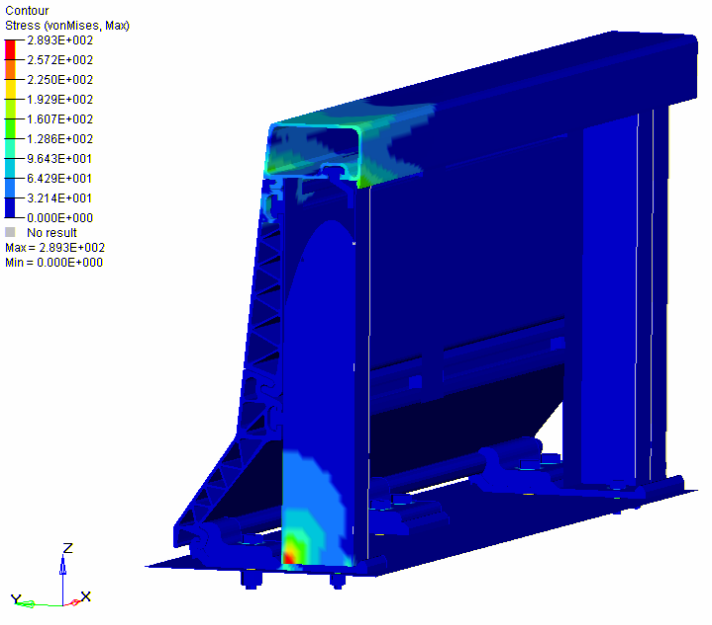

Figure 36. Effective stress contours at the cross-section through the post for the AASHTO LRFD vertical centered-on-mid-span test level four load case.

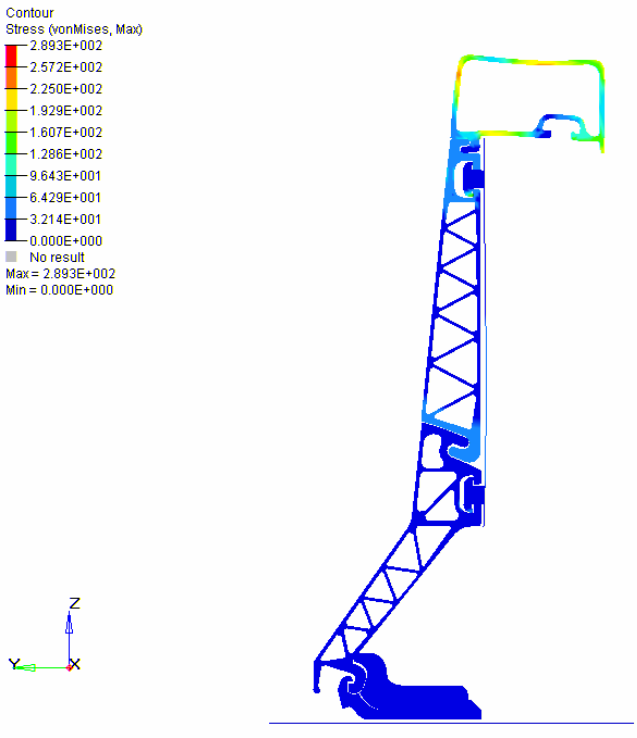

Figure 37. Effective stress contours through the cross-section of maximum vertical deflection for the AASHTO LRFD vertical centered-on-mid-span test level four load case.

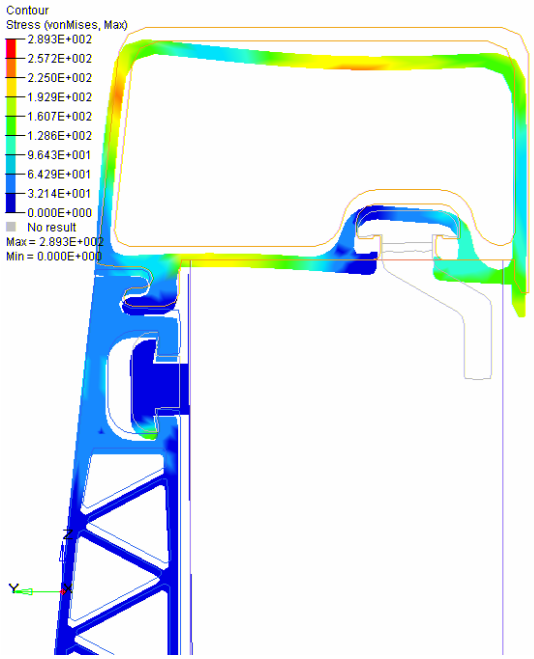

Figure 38. Effective stress contours and deformations of the top rail through the cross-section of maximum vertical deflection for the AASHTO LRFD vertical centered-on-mid-span test level four load case.

Conclusions

The foregoing analyses have demonstrated by the use of the non-linear dynamic finite element program LSDYNA that both the aluminum parapet bridge railing and the aluminum median barrier can withstand the Test 3-11 pickup truck loading and only sustain minor deformations. The integrity of the barriers was maintained throughout the loading and only minor localized permanent deflections resulted. Most of the material in both barriers behaved elastically indicating that there was considerable reserve capacity. The aluminum parapet bridge railing and the aluminum median barrier can be considered essentially rigid F-shape barriers and since rigid F-shape barriers are widely considered to satisfy Report 350 test level three, these barriers should be considered test level three barriers as well.

The AASHTO LRFD procedure was also followed to evaluate the aluminum bridge parapet for test level four conditions. The quasi-static analyses showed that the barrier contains sufficient strength to resist the loads that would be expected in a test level four impact. In all cases, the barrier deformations, material stress and other structural performance parameters were acceptable and, in fact, showed that the barrier has considerable reserve capacity even in test level four conditions.

For both the dynamic test level three analysis and the quasi-static AASHTO LRFD test level four analysis, the barriers remained intact, experiencing only minor deformations and reasonable local deformations. The barriers perform essentially rigidly since in all cases the dynamic deflections are under 50 mm, usually significantly less. Since the barriers behave rigidly, it is reasonable to expect that they will perform much like other crash-tested essentially rigid F-shape barriers. Crash tests with the aluminum bridge parapet railing and the aluminum median barrier are very likely to result in acceptable performance in both test levels three and four conditions.

References

1. C. E. Buth, T. J. Hirsch and C. F. McDevitt, “Performance Level 2 Bridge Railings,” Transportation Research Record 1258, Transportation Research Board, Washington, D.C., 1990

2. M. E. Bronstad, L. R. Calcote and C. E. Kimball, Concrete Median Barrier Research, Report FHWA-RD-77-4, Federal Highway Administration, Washington, D.C., 1976.

3. H. E. Ross, Jr., D. L. Sicking, R. A. Zimmer and J. D. Michie, “Recommended Procedures for the Safety Performance Evaluation of Highway Features,” Report 350, National Cooperative Highway Research Program, Washington, D.C., 1993.

4. AASHTO, “AASHTO LRFD Bridge Design Specifications,” SI Units, 2nd ed with interim specifications through 2000, American Association of State Highway and Transportation Officials, Washington, D.C., 1998

5. F. G. Wright, “Bridge Rail Analysis,” FHWA Memorandum, Federal Highway Administration, Washington, D.C., 16 May 2000.

6. C. E. Buth *et al*, “Safer Bridge Railings,” Vol. I, FHWA Technical Report No. FHWA-RD-82-072, Federal Highway Administration, Washington, D.C., June 1984.

7. P. Tiso, C. A. Plaxico and M. H. Ray, "An Improved Truck Model for Roadside Safety Simulations: Part II -- Suspension Modeling," Transportation Research Record No. 1797, Transportation Research Board, Washington, D.C., 2002

8. F. Orengo, C.A. Plaxico and M. H. Ray, "Modeling Tire Blow-out in Roadside Hardwarew Simulations Using LS-DYNA," *Proceedings of the Annual Meeting*, American Society of Mechanical Engineers, Reston, VA, 2003.

9. E. Oldani, Study of a New Aluminum Bridge Railing Design for Suspended Bridges, Thesis, Department of Areospace Engineering, Politecnico di Milano, Milan, Italy, November 2003.